communications earth & environment

ARTICLE

https://doi.org/10.1038/s43247-023-00936-w OPEN

# Recycled carbonates elevate the electrical conductivity of deeply subducting eclogite in the Earth's interior

Chenxin Jing [1,2], Haiying Hu[1]✉, Lidong Dai[1], Wenqing Sun[1], Mengqi Wang[1,2] & Ziming Hu[1,2]

The elevated pressure and temperature conditions encountered by a subducted slab entering the deep Earth can substantially alter the chemical composition and physical properties of recycled carbonates. Carbonate-silicate reactions are believed to have a pivotal role in this process. Here we conduct high temperature and high pressure experiments on carbonated eclogite and measure the electrical conductivity in order to constrain the evolution of geophysical properties and chemical composition in the carbonate-bearing eclogitic slab. We find that the carbonate-silicate reaction elevates the conductivity of carbonated eclogite by cations (e.g., Ca, Mg, Fe) exchange between carbonates and silicate. We propose that carbonate-silicate cations exchange can alter the chemical composition of recycled carbonates, potentially impacting their stability and reducing the solidus temperature of carbonate-bearing systems. Combining thermodynamic calculations with the elevated conductivity in our experiments, we re-evaluate the contribution of recycled carbonates to the Earth mantle geophysical anomalies and obtain the potential carbonate capacity in the subducting slab.

[1] Key Laboratory of High-Temperature and High-Pressure Study of the Earth's Interior, Institute of Geochemistry, Chinese Academy of Sciences, Guiyang 550002 Guizhou, China. [2] University of Chinese Academy of Sciences, 100039 Beijing, China. ✉email: huhaiying@vip.gyig.ac.cn

Recycled carbonates via the down-going altered oceanic crust into deep Earth are inevitably regarded as an essential carbon sink[1–4]. Carbonates in subduction zones originates from the oceanic sediments, serpentinites, altered oceanic crust, and suboceanic mantle lithosphere[1,2]. A part of them was devolatilized or stagnated at relatively shallower depths (~50 km in the hot subduction zone and ~100 km in the cold subduction zone), while the residual carbonates was sequestrated in the eclogitic slab into deep mantle further. Decarbonation (metamorphism, carbonate dissolved[5,6], and carbonate molten[4,7–9]), carbonate stagnation, and carbonates deep subduction decide the deep Earth carbon cycling paths and flux as a research hotspot in the last decade[1–4,6,8–25]. Until now, details of these procedures are still exploring constantly.

For the stability of single carbonate under high-pressure and high-temperature conditions, dolomite $CaMg(CO_3)_2$, magnesite $MgCO_3$, and calcite $CaCO_3$ can survive in the deep Earth mantle[26–28]. However, after experienced carbonate-silicate interactions in the eclogitized slab[15,16,29], physicochemical properties (e.g., chemical composition and electrical conductivity) of these carbonates can be perturbed. However, in contrast to the carbonate dissolution and melting occurring in the shallow hydrothermal environment of the subduction zone, the impact of carbonate-silicate interactions (e.g., cations exchange) which take place in all stages of slab subduction before carbonate melting is still not explicit in the Earth's interior. Tao and Fei[15] conducted a series of experiments focusing on redox reactions between majoritic garnet and carbonates in the lowermost upper mantle. However, there is still a lack of understanding whether other carbonate-silicate interaction (e.g., cations exchange and redox reactions) has been existed in the subducting slab from Earth's surface to deep Earth. The carbonate-silicate reactions at the lower mantle has been uncovered[16,28]; nevertheless, it is too doubtful whether pure carbonates ($CaCO_3$ or $MgCO_3$) like on the Earth surface are carried down after going through the subduction zone. Also, the Fe-bearing carbonates (Fe-dolomite, Fe-magnesite, and Fe-calcite), possibly caused by carbonate-silicate cations exchange, often occur in the many carbonated rocks (e.g., natural carbonated eclogites), whereas the origin and influence of these carbonates rarely are attained more attention yet[29–31]. Thus, the carbonate-silicate interaction and its impact in deeply subducting eclogitic slabs should be figured out distinctly.

From geological investigations, most carbonates host in some subducted rocks, typically natural (hydrous) carbonated eclogite[29,30,32–41], which by exhumation provide a direct observation of recycled carbonates in the Earth shallow depths (<~100 km). Experimental studies on the solidus of dry carbonated eclogite reveal the maximum subducting depth of recycled carbonates in the eclogitized slab before carbonates melting in the Earth's interior, and has provided clues to the evolution of carbonate-bearing system in the deep Earth (depth >150 km)[42–46]. We conducted electrical conductivity experiments and revealed carbonate-silicate reactions at high temperature and high pressure by adding dolomite, calcite, and magnesite in a relatively dry eclogite (no hydrous minerals), respectively, to explore geophysical peripeties and chemical composition evolution of the carbonate-bearing eclogitic slab. Three types of dry carbonated eclogite (dolomite + eclogite, magnesite + eclogite, and calcite + eclogite) were constructed to investigate their electrical conductivity and chemical composition evolution under elevated conditions. Different types (dolomite, calcite, and magnesite) and content (10–40 wt%) of carbonates were added in the eclogite, which were referenced to the mineral proportions and the bulk chemical composition of natural carbonated eclogites[30–32,47] and starting materials and recovered products of high-pressure and high-temperature experiments[43–46,48] (Fig. 1 and Supplementary Note 1).

## Results

**Carbonate-silicate cations exchange**. Carbonate-silicate cations exchange was uncovered through analyzing recovered products after in situ electrical conductivity (EC) measurements of carbonated eclogites, which may be an essential carbonate-silicate reaction in the deeply subducted slab. Three types of carbonated eclogite, including dolomite + eclogite, calcite + eclogite, and magnesite + eclogite, were employed in our EC experiments, to obtain the conductivity and explore the thermochemical evolutions of measured system at 3 GPa and up to 1200 °C. Upon comparing pre-sintered samples before EC measurements and recovered products after EC measurements (Fig. 2a, b and Supplementary Fig. 1a), severe reactions between dolomite and silicates (garnet and omphacite) in the recovered dolomite eclogites produced metamorphic features. Concretely, carbonate-silicate cations (Ca, Mg, Fe) exchange, induced by chemical potential gradients between carbonates (dolomite, calcite, and magnesite) and silicates (garnet and omphacite) in metastable assemblages (Fig. 2b–d and Supplementary Fig. 1b–f), plays a key role. Despite a small amount of water (or hydrogen) in the crystal lattice of the garnet and omphacite (Supplementary Note 2), it is worth noting that we ignore the potential impact and process of inter-diffusion of trace elements, like $H^+$ or $OH^-$.

EC experiments of dolomite-bearing eclogites were carried out, including 10, 20, 30, and 40% dolomite + eclogite as starting material. A garnet reaction zone is observed in the all recovered products texture (Fig. 2b and Supplementary Fig. 1c–e), which may be caused by Fe-Mg exchange between dolomite and garnet:

$$CaMg(CO_3)_{2(Dol)} + Fe_3Al_2(SiO_4)_{3(Grt)} \rightarrow Ca(Mg,Fe)(CO_3)_{2(Dol-Ank_{ss})} + (Mg,Fe)_3Al_2(SiO_4)_{3(Grt_{ss})} \quad (1)$$

Dolomite received Fe from garnet and released Mg to it; as a results, the FeO content of the dolomite-ankerite solid solution increase from near zero in the starting dolomite to ~4–8 wt% in the recovered dolomite (Supplementary Data 1). On the other hand, Fe-Mg exchange between dolomite and omphacite also increased the FeO content of the dolomite:

$$CaMg(CO_3)_{2(Dol)} + CaFeSi_2O_{6(Omph)} \rightarrow Ca(Mg,Fe)(CO_3)_{2(Dol-Ank_{ss})} + Ca(Mg,Fe)(Si_2O_6)_{3(Omph_{ss})} \quad (2)$$

Electron probe microanalyzer (EPMA) element maps display details of the exchange and diffusion for Si, Ca, Mg, and Fe (Supplementary Fig. 2). A visible Ca concentration gradient, from the core and mantle to the rim of the recovered dolomite, suggests that a part of Ca diffused into the neighboring garnet (Supplementary Fig. 2c), possibly generated by moderate Ca-Fe exchange between dolomite and garnet:

$$CaMg(CO_3)_{2(Dol)} + Fe_3Al_2(SiO_4)_{3(Grt)} \rightarrow (Ca,Fe)MgCO_{3(Dol-Ank_{ss})} + (Ca,Fe)_3Al_2(SiO_4)_{3(Grt_{ss})} \quad (3)$$

Ca-Fe exchange, thus, also could promote the formation of Fe-dolomite.

EC experiments on magnesite-bearing eclogite were also conducted, setting 10 wt% and 20 wt% magnesite + eclogite as initial assemblies, respectively. For the recovered magnesite eclogite (Fig. 2d–i and Supplementary Fig. 1f–i), its garnet reaction zone is similar to the dolomite eclogite (Fig. 2b and Supplementary Fig. 1c–e); accordingly, magnesite composition was enormously transformed from $MgCO_3$ in the starting materials to $Fe_{0.8-0.14}Mg_{0.42-0.39}Ca_{0.50-0.47}CO_3$ in the recovered products (Supplementary Data 1). Combined with BSE images, elemental maps,

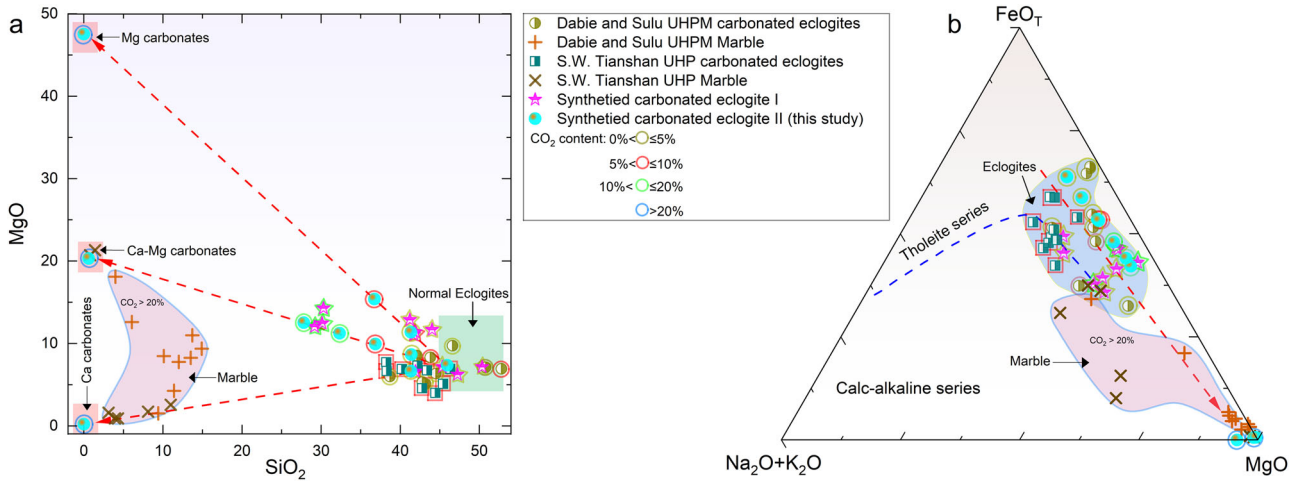


**Fig. 1 Chemical compositions of carbonated eclogites. a** MgO versus $SiO_2$ plot displays the distinction of the bulk composition of natural carbonated eclogites and marbles, synthetized carbonated eclogites, and normal eclogites. **b** AFM diagram[129,130] of carbonated eclogites. These carbonated eclogites are tholeiitic and likely formed from subducted basaltic oceanic crust. Natural carbonated eclogites and marbles are found in the Southwestern Tianshan UHP belt, NW China[30–32,47], and the Dabie-Sulu UHPM belt, E China[41]. Synthetized carbonated eclogite I is the starting material composition in HT-HP simulation experiments[42–46,48]. Three types of carbonated eclogite (synthetized carbonated eclogite II) bearing different types and content of carbonates (dolomite, calcite, magnesite) were constructed for this study (Supplementary Tables 2 and 3). The light green area represents the compositional distribution of normal eclogites in (**a**)[129]. Each sample bearing carbonates is covered by hollow shells of different colors that indicate the range of $CO_2$ content. Red dash lines with the arrow direct the increasing carbonation of eclogite.

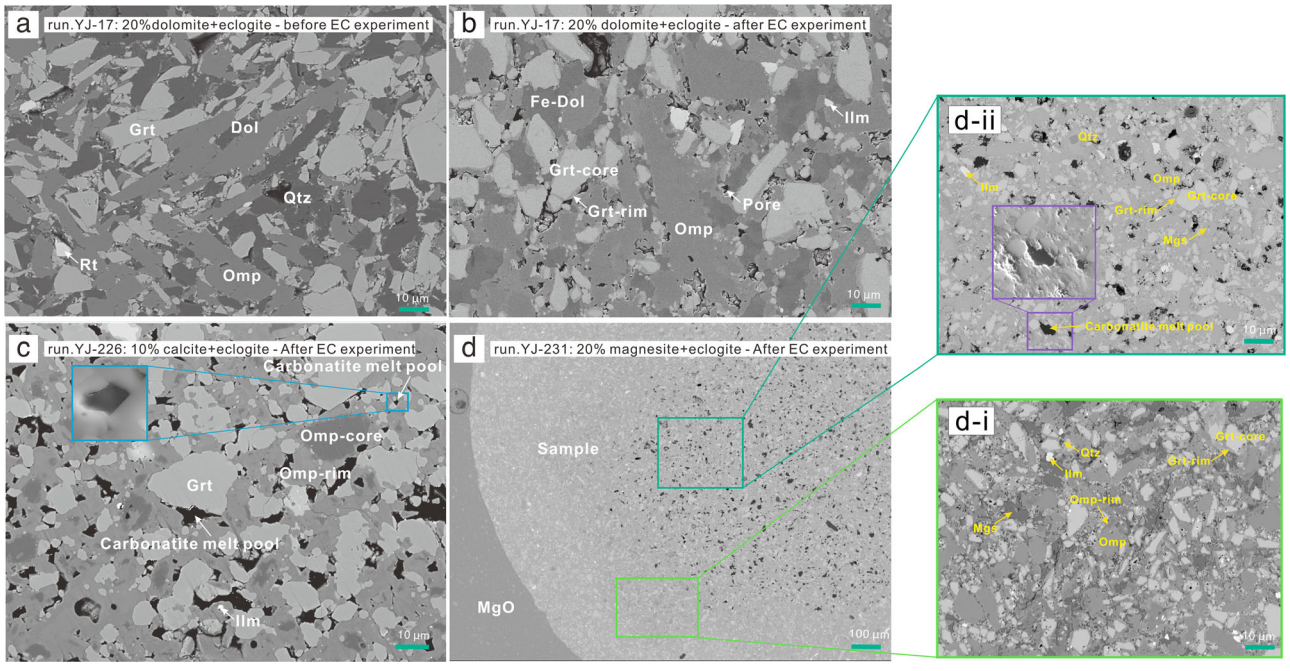


**Fig. 2 Experimental products at high pressure and high temperature.** Representative backscattering electron (BSE) images of mineral assemblages on 20% dolomite + eclogite before (**a**) and after (**b**) the EC experiment (YJ-17), including garnet (Grt), omphacite (Omp), dolomite (Dol), quartz (Qtz), and rutile (Rt) or ilmenite (Ilm). Pores were produced due to the slight devolatilization during the reaction between dolomite and silicates (Grt and Omp). Garnet reacts with dolomite to form a reaction zone (garnet rim) when its electrical conductivity tended to be repeatable (Supplementary Fig. 6b). **c** Typical BSE image of 10% calcite + eclogite after EC experiment (YJ-226). Carbonate melt pool appeared when its electrical conductivity tended to be repeatable (Supplementary Fig. 6d). A typical SE (the second electron) image presents the carbonate melt pool in the system. In these mineral assemblages, the addition of calcite significantly changes the composition of Omp (Supplementary Data 1), leaving only a small amount starting omphacite (Omp-core). **d** A global BSE image of 20% magnesite + eclogite after EC experiment (YJ-231). It also displays the partial melting of magnesite (Mgs) in the system when the conductivity tended to be repeatable (Supplementary Fig. 6e). **d**-i A typical reaction area of Mgs and silicates (Grt and Omp). **d**-ii A typical partial melting zone of magnesite in the center of the sample and an SE image showing the carbonate melt pool details.

and EPMA data (Fig. 2d–i, Supplementary Fig. 3 and Supplementary Data 1), the modification of magnesite composition could be traced by Fe-Mg and Ca-Mg exchange between magnesite and silicates:

$$MgCO_{3(Mgs)} + (Fe,Ca)_3Al_2(SiO_4)_{3(Grt)} \rightarrow (Ca,Fe,Mg)CO_{3(Mgs-Ank_{ss})} + (Ca,Fe,Mg)_3Al_2(SiO_4)_{3(Grt_{ss})} \quad (4)$$

$$Mg(CO_3)_{2(Mgs)} + CaFeSi_2O_{6(Omph)} \rightarrow (Ca,Fe,Mg)CO_{3(Mgs-Ank_{ss})} + Ca(Fe,Mg)(Si_2O_6)_{(Omph_{ss})} \quad (5)$$

where Ca and Fe in garnet and omphacite substitute for parts of Mg in magnesite to form iron-calcium-magnesium carbonate solid solutions (Mgs-Ank$_{ss}$). Notably, Ca in the solid solutions mainly comes from omphacite, and Fe mainly derives from Garnet (Supplementary Fig. 3).

We also performed the EC experiment of 10 wt% calcite + eclogite. However, the recovered calcite in eclogite was melting when temperature up to 1200 °C (Supplementary Note 3). Based on the reactions between dolomite (or magnesite) and silicates and residual silicate reaction zone in recovered calcite eclogite texture, the calcite-silicate reaction was not negligible under thermal disequilibrium of calcite eclogite before calcite melting. What can be observed is that only a little starting omphacite (Omp-core) remained in the recovered products (Fig. 2c); In the omphacite reaction zone, the weight percent of CaO contents increased by ~ 2 wt% and the weight percent of MgO contents decreased by ~ 2 wt% (Supplementary Data 1), which may be caused by the Ca-Mg exchange between calcite and omphacite. Similarly, the garnet reaction rim lost ~2 wt% FeO and obtain ~ 2 wt% CaO. Hence, the same as dolomite and magnesite, calcite in the eclogite also could transformed into iron-calcium-magnesium carbonate solid solutions:

$$CaCO_{3(Cal)} + (Fe,Mg)_3Al_2(SiO_4)_{3(Grt)} \rightarrow Ca(Fe,Mg)(CO_3)_{(Cal-Ank_{ss})} + (Ca,Fe,Mg)_3Al_2(SiO_4)_{3(Grt_{ss})} \quad (6)$$

$$Ca(CO_3)_{2(Cal)} + (Fe,Mg)Si_2O_{6(Omph)} \rightarrow Ca(Fe,Mg)CO_{3(Cal-Ank_{ss})} + Ca(Fe,Mg)(Si_2O_6)_{(Omph_{ss})} \quad (7)$$

EPMA element maps give details of elements exchange and diffusion for Si, Ca, Mg, and Fe in calcite eclogite (Supplementary Fig. 4), and EPMA data indicate the negligible diffusion of Al, K, and Na (Supplementary Data 1). It should be noted that the validity of Eqs. (1)–(7) should be verified by some phase transformations of carbonates or silicates further, but this is beyond the scope of this study.

Three types of carbonates reacted with silicates uncover that the composition of carbonates evolved in the eclogite (Supplementary Note 4), and the participation of carbonates upset the thermochemical equilibrium of the initial normal eclogite. Figure 3 shows a data compilation of carbonate and garnet compositions in carbonated eclogites from this study and previous experiments, which reveals the evolution directions of carbonate compositions. The compositional fate of recycled carbonates following the slab subduction from shallow Earth to deep Earth may eventually move toward the iron-calcium-magnesium carbonate ($Ca_xMg_yFe_{1-x-y}CO_3$) before the carbonate melting (Fig. 3a and Supplementary Note 4.1). Meanwhile, the composition of silicates (e.g., garnet) also evolves with that of carbonates (Fig. 3b and Supplementary Note 4.2).

**Elevated electrical conductivity**. The electrical conductivity of the carbonated eclogite (dolomite eclogite, magnesite eclogite, and calcite eclogite) was measured in situ at 3 GPa and up to 1200 °C. The conductivity of all measured systems increases as a function of reciprocal temperature (Fig. 4a, b). The participation of carbonates elevated the conductivity of eclogite below the solidus of carbonated eclogites and carbonates. Commonly, carbonates have lower conductivity than eclogite (Fig. 4a, b and Supplementary Note 5.1), so the addition of carbonates would reduce the conductivity of eclogite based on mixing models of electrical conductivity for aggregates. However, a series of electrical conductivity of carbonated eclogites, including 10, 20, 30, and 40 wt% dolomite + eclogite, 10, 20% magnesite + eclogite, and 10% calcite + eclogite, suggest that carbonates facilitate the conductivity of the carbonated eclogites (Fig. 4a, b).

The enhancement of eclogite conductivity by added carbonates coincides with the carbonate-silicate cations exchange, differing from the previous research ascribed to the higher conductivity of carbonate melt[49–52]. Hence, carbonate types and contents varied in eclogite may affect their conductivity by different degrees and types of reactions between silicates and carbonates (Fig. 4a, b and Supplementary Note 5.2). By detecting the weight percent of FeO content in dolomites of the recovered products, we determined that the FeO content in recovered dolomite decreased from 8.11 wt%, 7.17 wt%, 5.19 wt%, to 4.47 wt% with the increase of dolomite content in eclogite from 10% to 40%, respectively (Supplementary Data 1). Correspondingly, the weight percent of MgO content in their garnet reaction zones are similar. Because of the increase in carbonate content following the decreases in garnet content and the total iron content in the measured constituents under laboratory experimental conditions, less weight percent of garnet needs to provide iron for more weight percent of dolomite, resulting in that the higher dolomite content was contained in eclogite and the lower iron was partitioned into dolomite. As a result, the repartition and the reduction of conductivity-sensitive cations (e.g., $Fe^{2+}$) makes the conductivity increase first and then decrease with the increasing carbonate content in eclogite (Fig. 4a). Also, the effect of carbonate types on the electrical conductivity of eclogite may be caused by the difference in the dominant cation exchange (or diffusion) between different carbonates and silicates (Fig. 4b), such as dolomite reacting with silicates to accept Fe and release Mg, magnesite accepting Ca and Fe to release Mg, and calcite accepting Mg and Fe to release Ca (Supplementary Figs. 2–4). Meanwhile, all calcite and partial magnesite melted in eclogite under our experimental conditions may also contribute to the promotion and difference in the conductivity of three types of carbonated eclogite (Supplementary Note 5.2).

**Electrical conductivity capture carbonate-silicate cations exchange**. Carbonate-silicate cations exchange enhancing the electrical conductivity of the carbonated eclogite at high pressure and temperature relies on two crucial factors: (1) Ionic diffusion between mineral grains and (2) conductivity-sensitive ions (e.g., $Mg^{2+}$ and $Fe^{2+}$) homogenization in measured samples. Specifically, the ionic diffusion between carbonate-silicate grains leads to the gradually increasing conductivity of the dry carbonated eclogites, and then cations homogenization sustains the result.

The conductivity of diffused cations, namely ionic conduction, contributing to the system conductivity could be expressed by the Nernst-Einstein relation[53]:

$$\sigma = \sum_i \frac{f_i D_i c_i q_i^2}{kT} \quad (8)$$

where $\sigma$ is the electrical conductivity, $f_i$ is the nondimensional formation factor for the $i$th species, $D_i$ is the diffusion coefficient

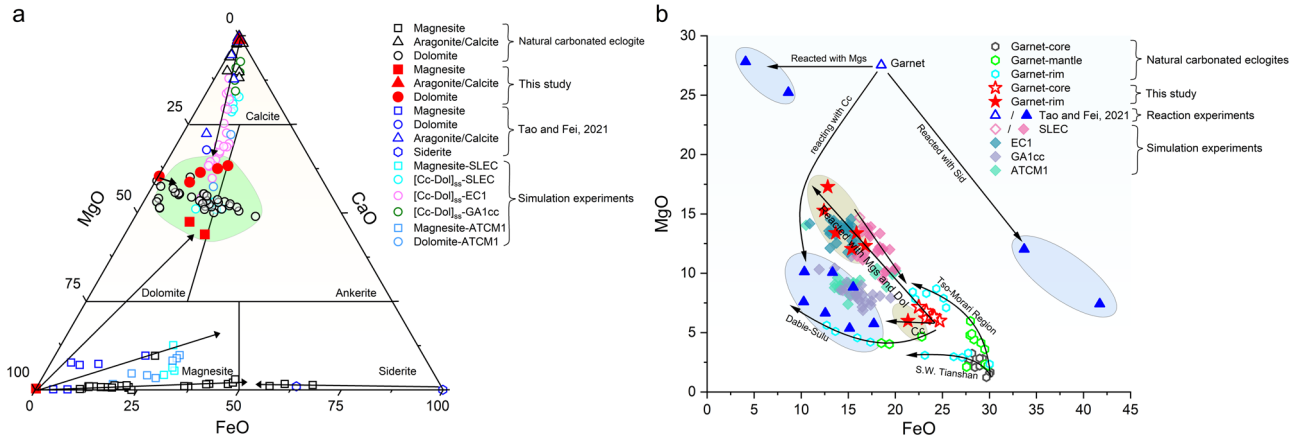


**Fig. 3 Compositional evolution of recycled carbonates and garnets.** The cations exchange (e.g. Mg-Fe) between carbonates and silicates altered their initial composition (Supplementary Note 4). **a** FeO-MgO-CaO ternary diagram shows composition trends of carbonates in the eclogite during slab subduction. Analyzing carbonates (dolomite, magnesite, and calcite) in eclogite from the field survey (natural carbonated eclogites)[30–32,34,40,47,67,74], laboratory simulation experiments (SLEC, EC1, GA1cc, and ATCM1 see Supplementary Table 2)[43–46,48], this study experiments, and the garnet-carbonates reaction experiments[15] determine the chemical composition fate of recycled carbonates. **b** Compositional evolution diagram of garnet in subducting carbonated eclogite. The diagram shows a compositional gradient, from garnet core, mantle, to rim in natural carbonated eclogite[30,31,34,47,67] and this study experiments products, which records the reaction between carbonates and garnet, providing an insight into a compositional direction of subducted garnet. Laboratory simulation experiments[43–46,48] and carbonate-silicate reaction experiments[15] suggest other possibilities for the composition evolution of recycled garnet. The increase in Fe and decrease in Mg in carbonate correspond to the decrease in Fe and the increase in Mg in garnet.

of the *i*th charged mobile species, $c_i$ is the concentration of the *i*th species, $q_i$ is the electrical charge of the *i*th species, and $k$ and $T$ are the Boltzmann constant and the absolute temperature, respectively. The potential ionic conduction may be crucial for increasing the electrical conductivity in different heating-cooling cycles (Fig. 4c and Supplementary Note 5.3). Taking 20% dolomite + eclogite as an example, the contribution of the ionic diffusion induced by carbonate-silicate cations exchange between dolomite and silicates to elevate electrical conductivity was recorded by the EC measurements in different heating-cooling cycles (Fig. 4c). The results show that the electrical conductivity of dolomite eclogite has considerable boost from the initial EC measurement cycle to the end cycle after conductivity-sensitive cations (e.g., $Fe^{2+}$, $Mg^{2+}$) experienced the diffusion between dolomite and silicates (garnet and omphacite) (Fig. 4c). With its correspondence, the activation enthalpy of the initial cycle conductivity to the end gradually decreases at low temperature (from 76 to 35.95 kJ/mol) and high temperature (from 115 to 63 kJ/mol), respectively (Fig. 4c, d). Finally, the cations diffusion between carbonate-silicate grains was weakened because the system gradually tended to reach chemical equilibrium in the dolomite. For other carbonated eclogites in this study, with the reaction between carbonates and silicates, their conductivity variation from the initial cycle heating to the end cycle cooling is similar to that of 20% dolomite + eclogite (Fig. 4c and Supplementary Fig. 5a, b). Nevertheless, the two experiments on magnesite eclogites are different (Supplementary Fig. 5c, d). The magnesite reacted with silicates and enhanced conductivity of magnesite eclogite in the first heating cycle. The end of the subsequent increase in electrical conductivity may be related to the formation of some low conductivity phase or slight devolatilization (Supplementary Note 5.2.3.1). Even so, the fact that the conductivity of magnesite eclogite increases with increasing magnesite content remains unchanged (Fig. 4b).

The trend of conductivity-sensitive ion homogenization in samples allow ions that were initially aggregated in a mineral (e.g., major $Fe^{2+}$ concentrated in garnet in a normal eclogite) to more widely partition into other minerals (e.g., the formation of Fe-bearing carbonates and Fe-richer omphacite) to be adequately distributed throughout a sample when the system tends to chemical equilibrium (Supplementary Figs. 2–4). Although, in most cases, the measured system only achieves local equilibrium as in this study, the diffusion of ions distributed from order to disorder provides potential opportunities to elevate the conductivity: (1) Multicomponent diffusion, specifically between carbonates and silicate, may reduce the activation enthalpy ($\Delta H$ in Eq. (9)) and consequently increase the electrical conductivity of measured samples (Fig. 4c, d); (2) It promotes the formation of some new high-conductivity phases (e.g., Fe-bearing carbonates and Fe-richer omphacite); (3) Even though the grain-boundary conduction subject to many factors, such as the concentration of hydrogen and the grain size (<10 μm), the increase in conductivity-sensitive ion concentration at the grains boundary may prompt the contribution of the grain-boundary conduction to the bulk conductivity of measured samples[54]. Therefore, the increase in the electrical conductivity of eclogite caused by carbonate-silicate cations exchange needs careful and comprehensive consideration (Supplementary Note 5.2).

The EC measurement tends to obtain the conductivity of a textual equilibrium sample via several heating-cooling cycles until they achieve remarkably consistency. Although we have made effort to measure the electrical conductivity of each sample to reach the apparent textural equilibrium as inferred from in situ conductivity measurement (Supplementary Fig. 6 and Fig. 4c), the observed microscopic textural of recovered samples are not a global equilibrium yet. According to our microscopic analysis, the recovered carbonates (e.g., dolomite) are close to chemical equilibrium, while the recovered silicates (e.g., garnet) exhibit a clear chemical potential gradient. Thus, we assume that the disparity is due to the cessation of carbonate-silicate cation exchange when the conductivity are consistent, whereas the cations self-diffusion of silicate (e.g., garnet) cations is still going on. For the case of 20% dolomite + eclogite (Fig. 4c), its conductivity gradually increase from the first heating cycle to the third cooling cycle due to the carbonate-silicate cations exchange, while its conductivity hardly change from third cooling cycle to the fourth cooling cycle, though the measured samples are not a global equilibrium. Specifically, the carbonate-silicate cations exchange can significantly

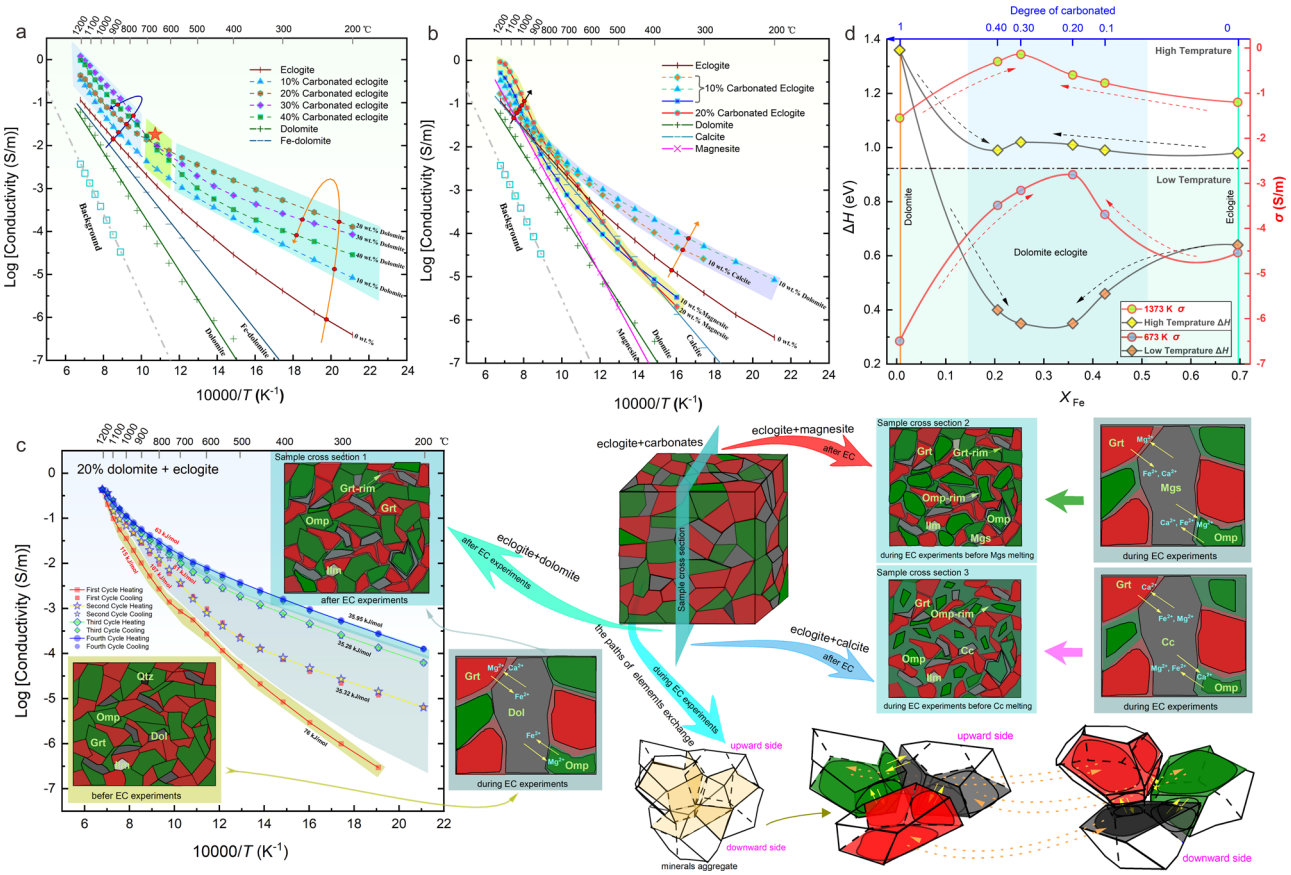


**Fig. 4 Electrical conductivity of three types of carbonated eclogites and the effect of carbonates-silicate cations exchange on it. a** Electrical conductivity of dolomite eclogite as a function of reciprocal temperature. Measured electrical conductivity of 10%, 20%, 30%, and 40% dolomite + eclogite, respectively. **b** Electrical conductivity of calcite eclogite and magnesite eclogites as a function of reciprocal temperature. Measured electrical conductivity of 10% calcite + eclogite, and 10% and 20% magnesite + eclogite, respectively. Also, the electrical conductivity of carbonated eclogite is compared to that of the initial eclogite, dolomite, Fe-dolomite, calcite, and magnesite as references in (**a**) and (**b**). The red star in (**a**) indicate a shift in electrical conductivity due to the variation of dolomite content in the eclogite. **c** The relationship between the elevated electrical conductivity of carbonated eclogites and the carbonates-silicate cations exchange. The schematic cube of carbonates + eclogite aggregates represent an carbonated eclogite assemblages. Three types of carbonated eclogites corresponds to three scenarios, i.e., dolomite + eclogite, calcite + eclogite, and magnesite + eclogite, respectively, showing details in the schematic sample cross-Sections 1-3 of the carbonated eclogite cube. Sample cross-Section 1 displays the schematic texture of dolomite eclogite after the EC experiment. The texture of 20% dolomite + eclogite experienced changes before, during, and after EC experiments in the heating-cooling cycles of EC measurement due to the carbonate-silicate reactions. Sample cross-Sections 2 and 3 illustrate the schematic texture of calcite and magnesite eclogite during EC experiments before calcite and magnesite melting, respectively, and show their elements exchange between carbonates and silicates. Schematic minerals aggregate displays the three-dimensional cations exchange paths between carbonates and silicates at the elevated condition. **d** $X_{Fe}$ (= wt% FeO/(MgO + FeO)) in dolomite of dolomite eclogites versus the activation enthalpies of the electrical conductivity at high and low temperature (left axis), and the $X_{Fe}$ versus the electrical conductivity at 673 K and 1373 K (right axis). Dolomite and eclogite are set as references to compare with the dolomite eclogites in (**d**). The red dashed arrows indicate the increase in electrical conductivity from dolomite or eclogite to dolomite eclogites, and the black indicate the decrease in activation enthalpies.

enhance the carbonated eclogite conductivity, but the cations self-diffusion of silicate has little effect on it. This is also supported by the effect of silicate composition on the electrical conductivity, i.e., the little difference of garnet or omphacite composition (e.g., Fe and Mg) may not significantly impact their conductivity[55]. Consequently, once the electrical conductivity of carbonated eclogite was measured by the cessation of carbonate-silicate cations exchange, even though silicate did not reach chemical equilibrium, the electrical conductivity of measured system will be close to that of the global chemical equilibrium system.

## Implications

**Cations exchange on carbonate stability in the Earth's interior.** The melting of magnesite and calcite in the eclogite during our experiments could shed light on the impact of cations exchange on the carbonate stability under elevated conditions (Fig. 2c, d and Supplementary Note 3). As usual, pure carbonates (e.g., $CaMg(CO_3)_2$, $CaCO_3$, and $MgCO_3$) in the previous high-temperature and high-pressure experiments have a high melting point[27,56–58], whereas several studies on the solidus of the carbonated eclogite or peridotite have shown that the melting point of carbonates in a silicate system is relatively lower[4,42–46,59] (Supplementary Fig. 7a). Although, as usual, carbonate melted earlier than silicates reducing the solidus of the carbonated eclogite and peridotite has been ascribed to several factors[43,44,48,60], such the composition of the bulk rocks (Supplementary Fig. 7b), the carbon content of the bulk rocks, and a dry or hydrous system, the nature (e.g., chemical composition) of carbonates itself deserves more attention.

We know that the composition of recycled carbonates evolves with the increasing temperature and pressure in the carbonated

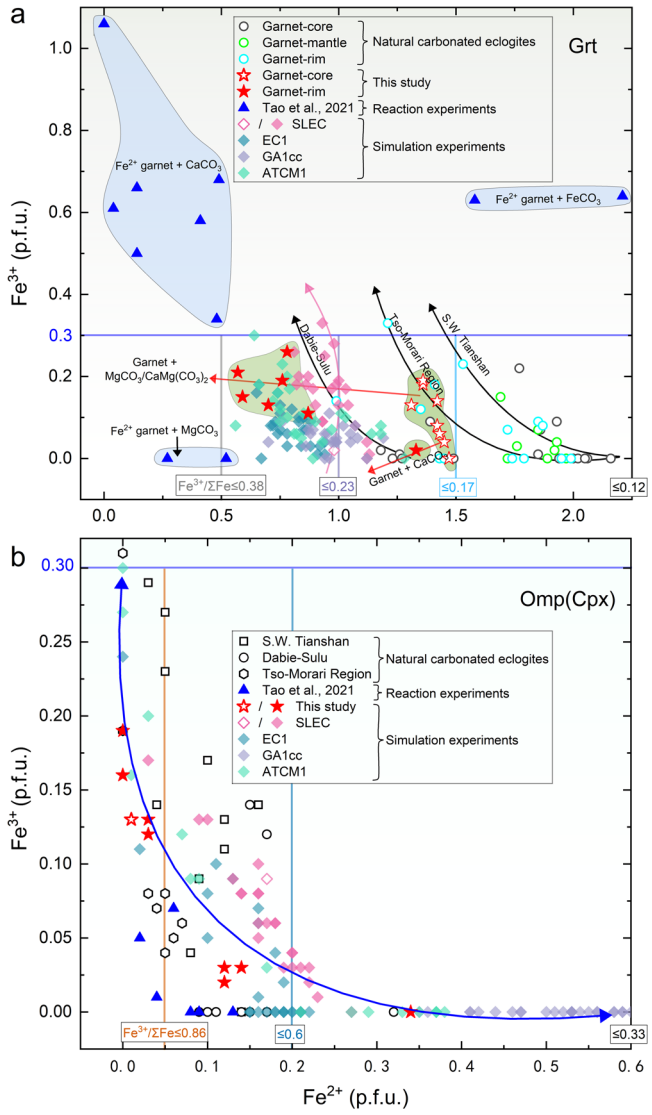


**Fig. 5 The $Fe^{3+}$ atomic number (p.f.u.) variation in major silicates of carbonated eclogites.** All garnets and omphacites (or clinopyroxenes) were collected from carbonate-bearing eclogites, including the field survey (natural carbonated eclogites)[30,31,34,40,47,67,74–76], laboratory simulation experiments (SLEC, EC1, GA1cc, and ATCM1 see Supplementary Table 2)[43–46,48], this study experiments, and garnet-carbonate reaction experiments[15], and then their chemical composition were recalculated (Supplementary Data 2). **a** $Fe^{2+}$ versus $Fe^{3+}$ in garnet (Grt) of carbonated eclogites. The $Fe^{3+}$ atomic number (p.f.u.) of the grain core, grain mantle, and grain rim of garnets from natural carbonated eclogites in the southwestern Tianshan UHP belt, NW China[30,31,40,47,67], the Dabie-Sulu UHPM belt, E China[74–76], and the UHPM of Tso-Morari Region, India[34] are tracked with black arrows. Using red and pink arrows direct the $Fe^{3+}$ atomic number (p.f.u.) of garnet's core (initial garnets) and garnet's rim (garnets reacted with carbonates) in this study and Dasgupta et al.[43,48], respectively. The $Fe^{3+}$ atomic number (p.f.u.) of garnets in other high-temperature and high-pressure simulation experiments serves only as the reference[44–46]. **b** $Fe^{2+}$ versus $Fe^{3+}$ in omphacite (Omp or Cpx) of carbonated eclogites. The blue arrow indicate the $Fe^{3+}$ atomic number (p.f.u.) range in the omphacite of carbonated eclogites. The $Fe^{3+}/\Sigma Fe$ ratios range is labeled at a specific $Fe^{2+}$ atomic number in garnets and omphacites of carbonated eclogites when the $Fe^{3+}$ atomic number is 0.3.

eclogite (Supplementary Note 4.1). The composition variation of carbonates induced by the carbonate-silicate cations (mainly $Ca^{2+}$, $Mg^{2+}$, and $Fe^{2+}$) exchange may be a critical process highly related to its many physicochemical behaviors (e. g., stability) in the Earth's interior. According to the available data from carbonated eclogites, the composition of single-cation ($CaCO_3$, $MgCO_3$, and $FeCO_3$) or double-cation ($CaMg(CO_3)_2$) carbonates in a silicate system will eventually evolve into the iron-calcium-magnesium carbonate ($Ca_xMg_yFe_{1-x-y}CO_3$) (Fig. 3a). Previous experiments on the carbonate solidus have pointed out that carbonates with a particular Ca# (Molar Ca/(Ca + Mg)) = ~0.6) have a lower melting point[61–63], which is consistent with the behavior of carbonate in the carbonated peridotite and eclogite[48,60,64]. Besides, Yaxley and Brey[44] assumed that the newly added FeO and $Na_2O$ in carbonates also could affect carbonate melting temperature in carbonated eclogites, in which alkali ions (e.g., K and Na) could lower its melting temperature[65] and specific molar Fe/(Mg + Fe) ratio (~40–48) in carbonates also could reduce its melting temperature[66]. Other carbonate-bearing systems, such as carbonate–biotite gneiss, suggest that the presence of Ca–Mg–Fe carbonates enable to decrease its melting temperature[64]. Notably, the iron content of recycled carbonates in the eclogite increases considerably, so we assume that the increased iron may positively promote the melting of carbonates in a silicate system. In this study, the composition of magnesite and calcite in the eclogite moved toward the miscibility of Ca, Mg, and Fe (Supplementary Note 4.1). Perhaps a potential low melting point due to a particular composition of iron-calcium-magnesium carbonate caused the melting of calcite and magnesite in our experiments at a specific temperature and pressure.

In addition, the compositional change in recycled carbonates may be closely associated with their phase transition. Fe could prompt Fe-dolomite to decompose into magnesite (or siderite) and aragonite at high temperature and high pressure[67]. Phase transitions of dolomite can be regarded as a function of iron content at high temperature and high pressure[68–70]. Moreover, carbonate-silicate cations exchange may accelerate cations disorder in carbonates, affecting their phase stability as well[27,71,72].

**Carbonate-silicate reaction on the eclogitic slab redox status.** Recently, recycled carbonates have come into our view as an efficient oxidation agent, which can react with $Fe^{2+}$-bearing silicates (e.g., garnet) to lead to $Fe^{3+}$ sink in the Earth's interior[15,38,73]. However, recycled carbonates widely modifying the redox state of the Earth's mantle is debatable. With the combination of our experimental assemblages (eclogite + carbonates), thus, we collected primary silicates (garnets and clinopyroxenes) of carbonate-bearing eclogites to overwhelmingly explore variations in their $Fe^{3+}$ atomic number (p.f.u.) to trace their redox status and link it to the impact of carbonate-silicate reactions during eclogitic slab subduction (Fig. 5).

In a more general context, the effect of carbonate-silicate reactions on redox state may be minimal in comparison with Tao and Fei's scenarios (a carbonated Fe-rich peridotite system)[15] (Fig. 5a). In this study, we conducted HT-HP experiments on a normal eclogite with different contents and types of carbonates (Supplementary Table 3). Although carbonates intensely reacted with silicates to generate a distinct reaction rim or zone in silicates (e.g., garnet) in all our experiments, no obvious increase in $Fe^{3+}$ atomic number from garnet cores (initial garnet) to garnet rims (reacted with carbonates) was displayed in Fig. 5a. Dasgupta et al.[43,48] also carried out a series of experiments on the solidus of bearing-carbonate eclogite (SLEC) under higher temperature and

higher pressure than ours. Similarly, the introduction of carbonates into the eclogite did not significantly increase the garnet $Fe^{3+}$ content compared with their initial garnet (Fig. 5a). Other HT-HP experiments[44–46] used a mixture of oxide and carbonates to crystallize carbonated eclogites (EC1, GA1cc, and ATCM1)[44–46], which also attained a relatively low $Fe^{3+}$ atomic number (<0.3 p.f.u.) in the recovered garnets (Fig. 5a). Garnets in natural carbonated eclogites, which were taken from the southwestern Tianshan UHP belt, NW China[30,31,40,47,67], the Dabie-Sulu UHPM belt, E China[74–76], and the UHPM of Tso-Morari Region, India[34] (Supplementary Fig. 7a), had experienced the HT-HP metamorphisms to provide metamorphic features (e.g., garnet core, mantle, rim) for us to trace their redox status. Despite a complex phase assemblage (e.g., garnet, omphacite, carbonates, quartz, rutile, epidote, and amphibole), the variation of $Fe^{3+}$ atomic number from the garnet core, mantle to rim implies that these natural carbonated eclogites are still in a low redox state (Fig. 5a). In addition, the low $Fe^{3+}$ atomic number (p.f.u. < 0.3) of clinopyroxenes in these carbonate-bearing eclogites also agrees with their relatively reduced redox state (Fig. 5b). Notably, it is necessary to consider the effect of carbonate-silicate cations exchange on $Fe^{3+}/\Sigma Fe$ ratios to prevent the misperception on the redox degree of carbonate-bearing system (details see "Methods").

In conclusion, carbonates may slightly enhance redox state of carbonated eclogite and should not be considered as an inner Earth oxidation agent widely. Correspondingly, the change of the redox state, despite being a crucial factor (e.g., oxygen fugacity) for electrical conductivity as usual[77,78], will not be taken into account in the conduction mechanism of the carbonated eclogite (Supplementary Note 5.2).

**Geophysical anomalies and carbonate capacity in the deeply subducted slab**. The elevated electrical conductivity of dry carbonated eclogites induced by the carbonate-silicate cations exchange may reverse the conventional cognition that unmelted carbonates cannot contribute to the high conductivity of inner Earth electrical structure[79–81]. Additionally, carbonates are generally low wave velocity and density[50,82–85]. Thus, recycled carbonates following the subducted slab into deep Earth may result in Earth's interior geophysical anomalies (e.g., low-velocity and high-conductivity zones). It is found that the added carbonates in eclogites may have significant impact on the subducting eclogite geophysical peripeties (density, wave velocity, and electrical conductivity)[50,82,85]. In consequence, we comprehensively explored the density, wave velocity, and electrical conductivity of carbonated eclogites, which are mainly constrained by the carbonate content (0–40 wt%) and types (dolomite, magnesite, and calcite) in eclogite, the constitution of eclogite (dry high-Fe/low-Fe eclogite and hydrous eclogite), and carbonated eclogites in a hot or cold subduction zone (Fig. 6 and Supplementary Note 6.1).

Plate subduction companied by mass circulation between the Earth's surface and interior cause the mantle heterogeneity[86–89], so properties of subducted plate are significant to the inner Earth physicochemical anomalies[90–94]. In this regard, we try to link the geophysical features of subducting carbonated eclogites to the anomalies of the field geophysical inversions in the upper mantle (Fig. 6). Analyzing our calculations and experimental results (Supplementary Note 6.2), we find that dry eclogites with ~10–20 wt% carbonates (i.e., ~5–10 wt% $CO_2$) would coincide with geophysical anomalies (positive/negative-density, low-velocity, and high-conductivity zones) of the upper mantle (100–300 km) in hot and cold subduction zones (Fig. 6a–e); more carbonates (> ~20 wt %) may cause the exhumation and stagnation of subducting carbonated eclogite in the mid-lower crust or uppermost mantle to assist the geophysical anomalies of shallow Earth (<~100 km, Fig. 6a, b), such as the mid-lower crust magnetotelluric anomalies of Ladakh Batholith in India[95], Kazakh Platform in Tianshan[96], and Dabie-sulu in China[97] (Fig. 6e-i); and hydrous carbonated eclogites could contribute to the geophysical anomalies of the mantle wedge (Fig. 6a–d). Compared with the hot subduction zone in the upper mantle, the density of carbonated eclogites are generally higher than that of the cold subduction zone, and the conductivity are lower and the wave velocity are higher in the cold subduction zone. Thus, we suggest that carbonated eclogites in the cold subduction zones could carry more carbonate (maximum to ~30 wt%) into the deep mantle than in the hot subduction zones, which would produce the potential positive/negative-density, low-velocity, and high-conductivity zones in the deeper mantle (>300 km) (Fig. 6). Combined with the carbon cycle in the deep Earth[4,16,26,98–100], potential geophysical anomalies tied to the recycled carbonates in the Earth's interior are marked in Fig. 7. Given the above discussions based on the hottest and coldest subduction zone in this study, our results for a specific subducting slab can serve as upper and lower thresholds for the density, wave velocity, and electrical conductivity of its explicit geothermal gradient. Meanwhile, the impact of carbonate types and content and the chemical composition and mineral constitutes of a specific subducting slab on the contribution of inner Earth geophysical anomalies cannot be ignored as well (Supplementary Note 6.2).

According to our results, the density, wave velocity, and electrical conductivity of the dry carbonated eclogite are sensitive to the carbonate content. Specifically, the increasing carbonates in the subducting eclogites will reduce its density and wave velocity and increase its conductivity (Supplementary Note 6.2), which may be essential to bind the carbonate capacity in the deeply subducting eclogitic slab. The plate subduction is due to the negative buoyancy of the surrounding mantle, so an appropriate carbonate content is critical for its further subduction (Supplementary Note 6.1.1). Based on the lower bound ($\rho > 3.3$ kg/m$^3$) of the plate subduction in the upper mantle, the maximum carbon capacity of the dry eclogitic slab may be ~10–30 wt% in the hot and cold seduction zones (Fig. 6a, b and Supplementary Fig. 8). Considering the carbon recycling efficiency (~ 40–60 wt%)[1,6,17], the incomplete dehydration of subducting slab (i.e., bearing low-density hydrous minerals)[101,102], and the density of subducting slab higher than the surrounding mantle commonly[103], we suggest that the carbonate capacity in deeply subducted slabs is ~ 5–15 wt% (i.e., ~ 2.5–7.5 wt% carbon). Due to the diversities of geophysical inversion, it is relatively weak for the velocity and conductivity to constrain a specific carbonate/carbon capacity in the deeply subducted slab currently. However, they may support the density result by comparing them with the deciphered seismic and magnetotelluric signals (Fig. 6c, d and Supplementary Fig. 9).

## Experimental methods

**Starting materials**. A natural gem-grade eclogite from the Dabie-Sulu ultrahigh-pressure metamorphic belt in eastern China was used as the initial material. Its chemical composition was analyzed and compared with a normal eclogite, MORB, simple crust, and alt-MORB in Supplementary Table 1. The eclogite contains 54 wt% omphacite, 43 wt% garnet, 1.5 wt% coesite, and 1.5 wt% rutile according to mass balance calculations (using Supplementary Data 1) and microscopic observations (Supplementary Fig. 1a), which represent a deeply subducted eclogite[104]. The water content of single garnet and omphacite picked out from the natural eclogite is 922 ppm and 447 ppm (Supplementary Fig. 11a), respectively. Three kinds of natural water-poor carbonates (Supplementary Fig. 11b), including dolomite, magnesite, and calcite as carbon source in carbonated eclogites, is fresh and no alteration. The carbonated eclogites were synthesized by

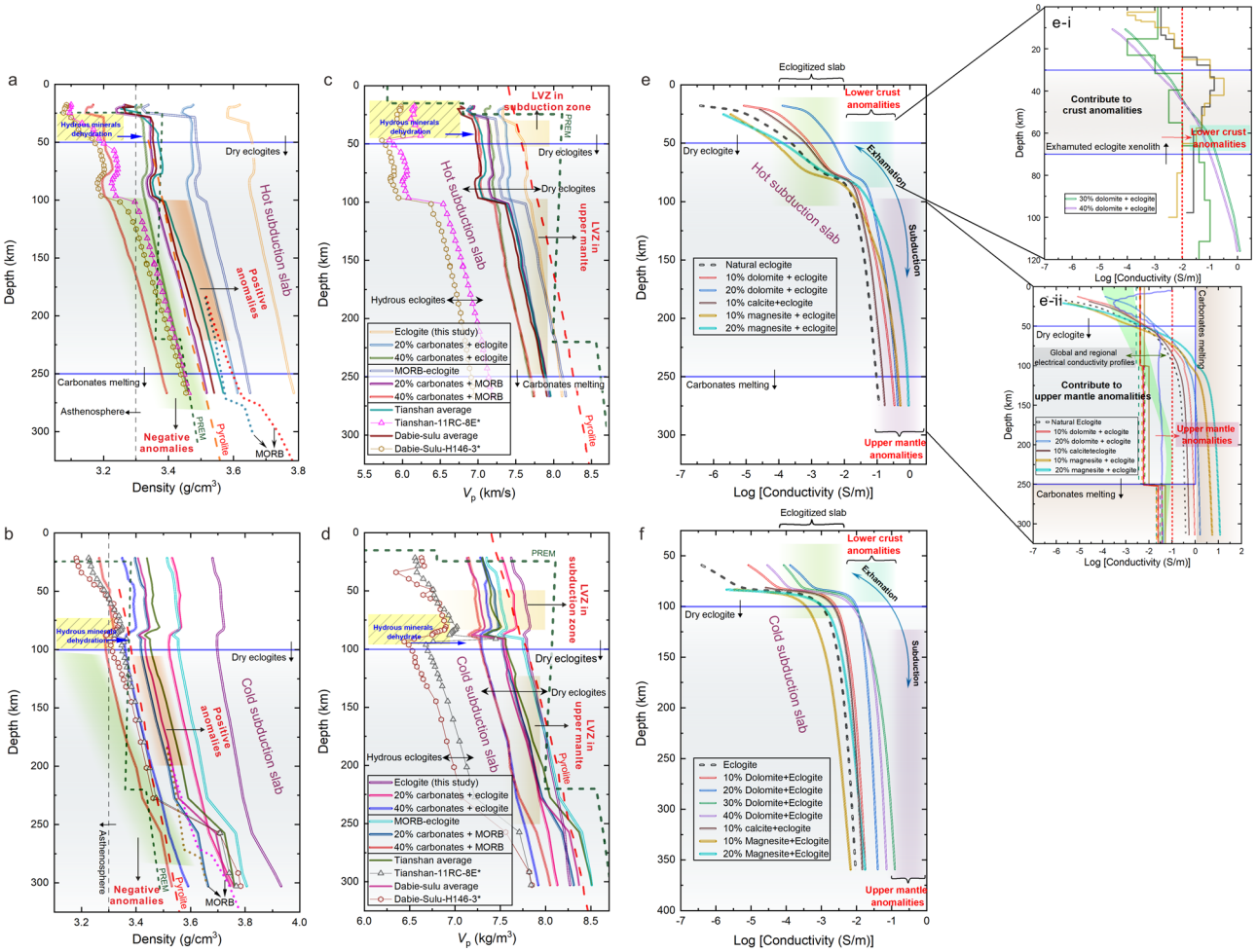


**Fig. 6 Geophysical profiles of carbonated eclogites. a–d** Density and P-wave velocity profiles for carbonated eclogites calculated along the hottest and coldest subduction zone geotherms[122,123] using Perple_X 6.9.014. Dry eclogite is associated with the deeply subducting eclogite (depth > ~ 50 km in the hot subduction zone and depth >~100 km in the cold subduction zone), and the hydrous eclogite represents a shallowly subducting eclogite; the presence of hydrous minerals, such as amphibole and epidote, distinguishes one from the other (Supplementary Table 4). Two eclogites, the low-Fe composition (MORB[131]) and high-Fe composition (this study), are considered to the impact of the eclogite composition on the density and wave velocity of carbonated eclogite; how much carbonates content is carried by different subducted eclogites into the deep Earth. The term "20% or 40% carbonates + eclogite (or MORB)" refers to the arithmetical average density and P-wave velocity of dry eclogite (low-Fe or high-Fe) containing either 20% or 40% dolomite, magnesite, and calcite eclogites, respectively (details see Supplementary Figs. 8 and 9). The term "Dabie-sulu (or Tianshan) average" refers to the arithmetical average density and P-wave velocity of dry natural carbonated eclogites from Dabie-sulu and Western Tianshan, respectively. This paper focuses on dry carbonated eclogites, but hydrous natural carbonated eclogites (11RC-8E* from Dabie-sulu and H146-3* from Western Tianshan in (**a**–**d**)) as references. The density of PRAM[132], MORB eclogite[133], pyrolite[134], and the P-wave velocity of PRAM[134] and pyrolite[135] are also as references. The yellow shaded areas present where hydrous mineral in hydrous eclogite undergo dehydration, while blue arrows show how density or P-wave velocity changes from the hydrous to dry systems in hot or cold subduction. Areas of density, velocity and electrical conductivity anomalies are delineated in (**a**–**d**) (details see Supplementary Note 6.2). **a**, **c** and **b**, **d** are the same legends, respectively. **e**, **f** Conductivity profiles for carbonated eclogites based on our EC experiments along a hottest and coldest subduction zone geotherms[122,123]. **e**-i Electrical conductivity profiles of exhumated carbonated eclogites along a 60 mWm$^{-2}$ continental lithosphere geotherms[136]. The crust conductivity anomalities ($\sigma > 2$ S/m) were labeled with a red dashed line. The magnetotelluric anomalities profile of Ladakh Batholith B-B′ in India[95], Kazakh Platform A-A′ in Tianshan[96], and Dabie-sulu A-A′ in China[97] were obtained (details in Supplementary Fig. 10), where carbonated eclogites were reported[30,32,34,41,74]. **e**-ii The electrical conductivity profiles of deep subducted carbonated eclogites along a 70 Ma upper mantle geotherms[137]. The electrical conductivity range ($-2.5$ S/m $<\log \sigma < -1$ S/m) of the global and regional mantle[138], the north Pacific and Philippine Sea mantle[139] are displayed, labeled with a two-way arrow. The shaded light-gray color area (50 km < depth < 250 km in hot subduction zone and depth >100 km in cold subduction zone) represents a ubiquitous region of a dry eclogite[140] and before carbonates melting[7].

mixing eclogite and carbonate powders in a series of mass ratios at high pressure and temperature (Supplementary Tables 2 and 3). It should be noted that no permissions were required for the samples used in this study.

Natural eclogite and carbonates (dolomite, Fe-bearing dolomite, calcite, and magnesite) were ground to 10–20 μm powder under ethanol in an agate mortar and pestle, respectively, then both of them were dried at 120 °C for 48 h to remove ethanol. Notably, the conductivity of silicate minerals by lattice conduction is independent of grain size[105,106], and the effect of grain size on the carbonate-silicate reactions is consistent across all of our experiments and did not pay more attentions. Mixtures of carbonates and eclogite based on a series of mass ratios were weighed for each starting material (Supplementary Table 3). Before loading into capsules, these mixtures are further ground under ethanol for 2 h to ensure significant homogeneous

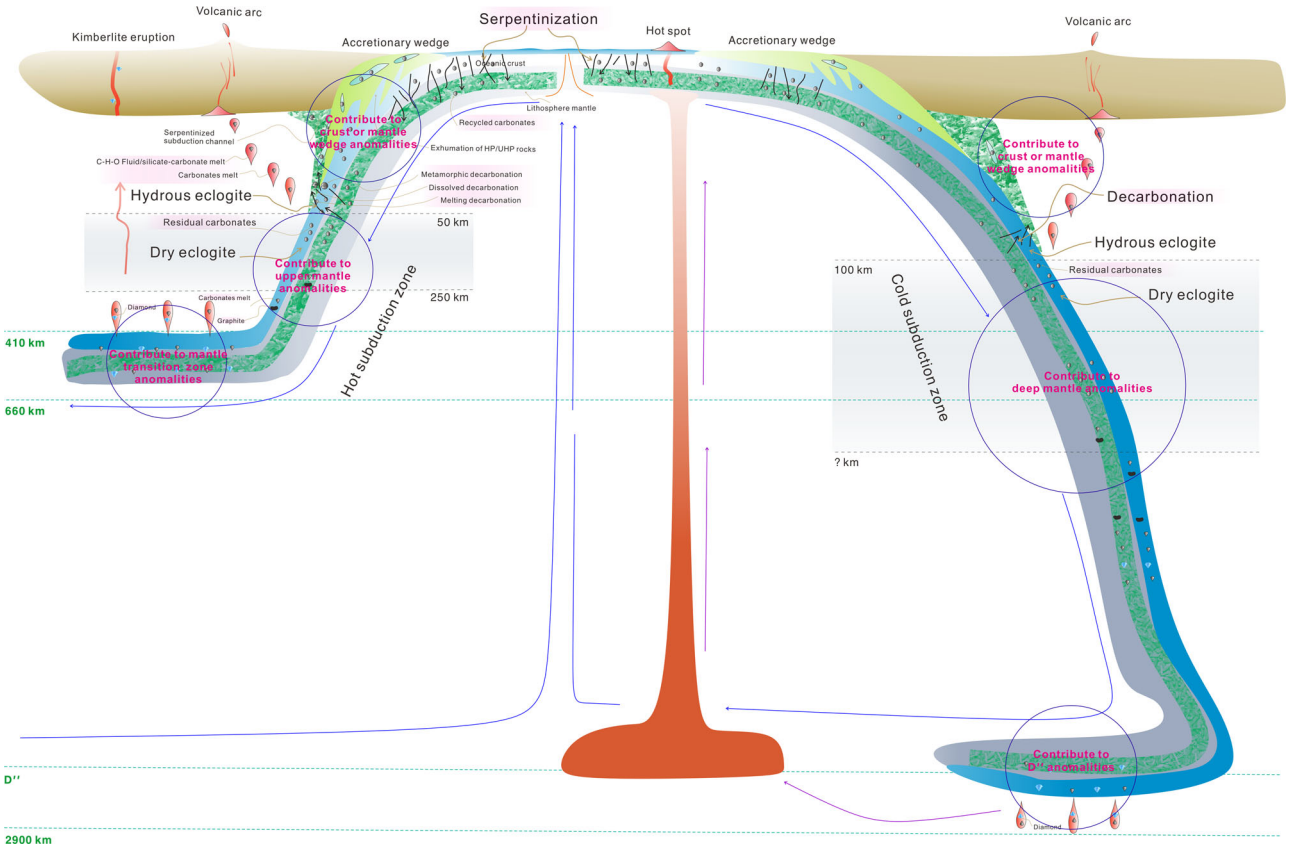


**Fig. 7 Recycled carbonates tied to potential geophysical anomalies in the Earth's mantle.** Two models depicting the subducted slab, including hot and cold subduction zone, exhibit different geothermal structures and subducted depths[103,141]. Recycled carbonates (e.g., dolomite, calcite, and magnesite) are injected into the subducting slab and lithosphere mantle through the serpentinization of the oceanic crust[142–147]. Once carried into the Earth's mantle via the two models of subducted slab, these carbonates undergo various process such as decarbonation (e.g., metamorphic decarbonation, dissolved decarbonation, and melting decarbonation)[6,11,148–151], reactions with silicates (e.g., cations exchange), melting[43,44,46], and phase transitions[152–154] under elevated conditions in Earth's interior. Ultimately, they are brought back to the Earth's surface due to erupted magma or mantle plume[155,156], completing the carbon cycle within the Earth's interior. Eclogite, formed by high-temperature and high-pressure metamorphism of basaltic oceanic crust, plays a crucial role as a carrier of carbonate to the deep Earth. Hydrous eclogites are associated with the decarbonation of carbonates as usua[16,157,158], while dry eclogites facilitate to the deep subduction of carbonates[43]. Based on our results and the carbon cycle within the Earth's interior[4,16,26,98–100], recycled carbonates may potentially contribute to geophysical anomalies, such as low density, low velocity, and high conductivity in the two subduction models, as indicated by purple circles. The shaded light-gray color area (50 km < depth < 250 km in hot subduction zone[7,140] and 100 km <depth in cold subduction zone[28]) represents a ubiquitous region of dry eclogites and carbonates before melting.

distribution of minerals in the bulk rock, then dry at 120 °C for 48 h to remove ethanol again, and their chemical composition was compiled in Supplementary Table 2. After the above procedures, each mixture was loaded into a Ni-lined Cu capsule (ID 6 mm, OD 6.3 mm, and length 13 mm). These capsules proceeded to hot-press at 3 GPa and 700 °C for 300 min using a YJ-3000t multi-anvil apparatus installed at the Institute of Geochemistry, Chinese Academy of Sciences, Guiyang, China, and its experimental assemblies are displayed in Supplementary Fig. 12a. The recovered samples were cored into cylindrical shapes of 5 mm diameter and 4 mm length for subsequent EC experiments.

**In situ electrical conductivity measurements**. In situ electrical conductivity measurements on carbonate-bearing eclogites were executed in the YJ-3000t multi-anvil apparatus at 3 GPa and up to 1200 °C using pyrophyllite pressure medium and stainless-steel sheets heater (Supplementary Fig. 12b). The hot-pressed sample was placed in MgO and $Al_2O_3$ sleeves for insulation from the stainless-steel sheets heater and was sandwiched between Ni electrodes. A piece of 0.025 mm thick nickel foil grounding as a shield layer was curled between the MgO and $Al_2O_3$ sleeves to avoid interference for conductivity measurements by the current in the heater. Meanwhile, the Ni electrodes and Ni foil served as Ni-NiO buffer to control the oxygen fugacity of the sample, corresponding to the redox condition within 200 km depth of subduction slab[107]. Two nickel-aluminum ($Ni_{97}Al_{13}$) thermocouples were used as measuring wires, internally connected to the nickel electrodes at both ends of the sample and externally to the Solartron 1260 impedance/gain-phase analyzer. $Ni_{90}Cr_{10}$-$Ni_{97}Al_{13}$ thermocouples were electrochemically welded in spherical contact directly against the middle of the sample, monitoring real-time temperature of the measured sample in each experiment. Each sample in this study was subjected to a fixed pressure (3 GPa) and then undergoes several heating-cooling cycles (473–1473 K), at an interval of 50 K, to collect the impedance spectrum at desired temperature (Supplementary Fig. 13). Each recovered sample after EC measurements was used for subsequent petrological analysis. In each conductivity measurement, the complex impedance spectra were recorded through the impedance analyzer by frequency sweeping at $10^6$–$10^{-1}$ Hz, and 1 V applied alternating voltage. The impedance spectrum was fitted by R-CPE (resistance-constant phase element) parallel circuit to obtain each

sample resistance $R$ using the impedance analysis software Z-View (Supplementary Fig. 13). The electrical conductivity were calculated by the formula $\sigma = L/SR$, where $L$ is the thickness of the sample (4 mm), and $S$ is the sectional area of the sample (diameter 5 mm). There is almost no deformation (less than 5%) in the recovered samples due to the experimental pressure of the samples is consistent with its prefabricated pressure. Under a constant pressure, electrical conductivity of measured samples experienced several heating-cooling cycles achieved remarkable consistency (Supplementary Fig. 6), which means that the measured sample almost tend to be textural equilibrium. The electrical conductivity ($\sigma$) of a sample is linearly dependent on the temperature ($T$), which is generally expressed by the Arrhenius formula:

$$\sigma = \sigma_0 \exp\left(-\frac{\Delta H}{kT}\right) \quad (9)$$

Where $\sigma_0$ is called the preexponential factor (a constant), $\Delta H$ is the activation enthalpy (J/mol or eV), and $k$ is the Boltzmann constant (J/K). Equation (9) was obtained for each sample through fitting the electrical conductivity of measured samples in this study (Supplementary Table 3), and its activation enthalpy linked to the conduction mechanisms of each sample (Supplementary Note 5).

**Analytical methods**. The chemical composition of eclogite was determined using a PANalytical Axios-advance (Axios PW4400) X-ray fluorescence spectrometer (XRF) at the State Key Laboratory of Ore-Deposit Geochemistry in the Institute of Geochemistry, Chinese Academy of Sciences, Guiyang, China. The initial samples and all recovered samples used in this study were embedded in epoxy resin to polish with diamond powders (3, 1, and 0.5 μm) for scanning electron microscopy (SEM) and electron probe microanalyzer (EPMA). Mineral compositional analyses (major element analyses and elemental maps) of each phase in our experiments, including omphacite, garnet, quartz, rutile, dolomite, Fe-bearing dolomite, calcite, magnesite, and melt glass (Supplementary Data 1), were performed using a JEOL JXA-8530F-plus Field Emission electron microprobe at the State Key Laboratory of Ore-Deposit Geochemistry in the Institute of Geochemistry, Chinese Academy of Sciences, Guiyang, China, under operating conditions of 10–25 kV accelerating voltage and a beam (1–10 μm) current of 5–10 nA with peak counting times in 100–200 s. BSE images were obtained by a FIB scanning electron microscope, a beam current of 1.6 nA, and a 10 kV voltage, at the Center for Lunar and Planetary Sciences, Institute of Geochemistry, CAS, Guiyang, China.

Trace water in minerals could significantly increase the electrical conductivity[108,109]. Garnet and omphacite are nominally anhydrous minerals but host a small amount of water (or hydrogen) in their crystal lattice[110]. Although this study centers the eclogite carbonation on the chemical composition evolution and geophysical properties, the intrinsic water content in garnet and omphacite as a crucial factor may affect the order of magnitude and conduction mechanism of the bulk rock's electrical conductivity[55,111,112]. Thus, garnet and omphacite were individually selected from natural eclogite aggregates used in this study for double-sided polishing to ≤150 μm thickness to detect their initial water by a Fourier transform vacuum infrared spectrometer (Vertex 70 V and Hyperion-1000 infrared microscope), with 50 × 50 μm aperture size to allow sufficient dozens of grains in the horizon, at the Key Laboratory of High-Temperature and High-Pressure Study of the Earth's Interior, Institute of Geochemistry, CAS, China. We obtained the infrared absorption spectra of garnet and omphacite by randomly selecting five spots in each sample with unpolarized light. (Supplementary Fig. 11a). Water contents in the natural garnet and omphacite were calculated by calibrated Beer-Lambert law with the infrared absorption spectra in the wavenumber range from 3000 to 4000 $cm^{-1}$:

$$C_{OH} = \frac{1}{\varepsilon\gamma}\int_{3000}^{4000}\frac{K(\nu)}{d}d\nu \quad (10)$$

where $C_{OH}$ is the water concentration (mol/l) in the targeted minerals; $K(\nu)$, a dimensionless quantity, is the absorption intensity (absorbance) of the water from the infrared absorption spectra[113]; $\varepsilon$, $\gamma$, and $d$ are the molar absorption coefficient (l/mol/$cm^2$), the orientation factor (a dimensionless quantity) that depends on crystallographic anisotropy and is 1/3 for the unpolarized IR spectra as usual, and the thickness of samples (cm), respectively. In addition, the infrared absorption spectra of two recovered samples and natural carbonates (dolomite, calcite, and magnesite) were also obtained to qualitatively determine whether these samples contain water (Supplementary Fig. 11b, c).

**Charge balance calculations**. Figure 5 shows $Fe^{2+}$ versus $Fe^{3+}$ plots of garnets and clinopyroxenes in the carbonated eclogites. The $Fe^{3+}$ atomic number (p.f.u.) is derived from the EPMA data via recalculating the formula of garnet and omphacite with the charge balance method[114]. Only using the charge balance method may bring some uncertainty about the accurate $Fe^{3+}$ content in garnet and omphacite without other assistance (e.g., the Mossbauer data), but enough data, i.e., more than 150 garnets omphacites, and carbonates participating in this study (Supplementary Data 2), may minimize the potential error.

The $Fe^{3+}/\Sigma Fe$ ratio, which characterizes the redox state of garnet in the carbonated eclogites, may overestimate or underestimate the role of carbonate as an oxidation agent in the Earth's interior. As is well known, both an increase in $Fe^{3+}$ and a decrease in $Fe^{2+}$ will enhance the $Fe^{3+}/\Sigma Fe$ ratio. The cations exchange between garnet and carbonates can either decrease or increase the iron content of garnet under elevated conditions (Fig. 3b). Thus, relying on the $Fe^{3+}/\Sigma Fe$ ratio to determine the redox state of a sample may not provide an accurate result. In this study, the $Fe^{3+}/\Sigma Fe$ ratio at the garnet rim is higher than the garnet core (Fig. 5a), which suggests a relatively higher oxidized state after reacting with carbonates. However, it is important to note that the decrease in $Fe^{2+}$ content of garnet is due to carbonate-silicate cations exchange, while its $Fe^{3+}$ content remains nearly unchanged. Tao and Fei15 reported strong oxidation of their $Fe^{2+}$-garnets after reacting with calcite and siderite (Fig. 5b), but they may have overlooked this fact (Fig. 3b). As a result, they exaggerated calcite as an oxidant and neglected siderite as a potential oxidant in their report (Fig. 5b). Consequently, we primarily investigate the variation of $Fe^{3+}$ atomic number (p.f.u.) in analyzing of the redox status of garnets, omphacites, and carbonates directly, and the $Fe^{3+}/\Sigma Fe$ ratio is used as an auxiliary tool, as shown in Fig. 5a, b.

**Thermodynamic calculations**. $P$–$T$ pseudosections for carbonated eclogites based on the chemical composition of bulk rock were drawn up with the software Perple_X package 6.9.1[115], which is based on a thermodynamic database (hp62ver.dat)[116]. Major elements of carbonated eclogites for the calculation compiled the chemical composition of eclogites (from XRF) and carbonates (from EPMA) across a series of mass ratios in Supplementary Data 3. According to the petrography of natural carbonated eclogites (hydrous) and dry carbonated eclogites in this study, Gt(WPH)[116], Omph(HP)[117], IIHm(A)[118], Do(HP)[116], Cc(AE)[119], and M(HP)[116], Amph(DPW)[120] and Ep(HP)[116] as solid solution models were applied in these thermodynamic

calculations (Supplementary Table 4). The carbonate-silicate reaction under elevated conditions may induce slight devolatilization ($H_2O$ and $CO_2$), so the compensated Redlich–Kwong (CORK) equation of state (EoS) was utilized for fluids[121]. The density and velocity of carbonated eclogites as a function of temperature and pressure were calculated using Perple_X 6.9.1 alongside the *P*–*T* paths of the hottest and coldest slab-top geotherms[122,123] after the pseudosection calculations. The density of the eclogitic slab may play a vital role in the subduction zone due the impact of the slab pull[124,125]. Generally, the density of eclogite is determined by mineral constituents, including the proportion of rich-Fe or poor-Fe garnet and omphacite[126,127] and the content of accessory minerals (e.g., carbonates, hydrous minerals)[82,125] in the bulk rock. These factors can affect that downgoing plates exhume to the shallow Earth crust, stagnate in Earth's interior, or subduct into the deep mantle[61,125,126,128]. The carbonation of eclogite can decrease its density due to the lower density of carbonates[85], which could hinder its further subduction of the eclogitic slab. In addition, carbonates are generally low wave velocity that could result in low velocities of seismic waves in the Earth's interior[82–84]. Thus, we calculated the density and P-wave velocity of eclogites containing dolomite, calcite, and magnesite at varying proportions (0, 20%, and 40%) of carbonates (Supplementary Figs. 8 and 9). This could help us determine the amount of carbon that carried by an eclogitic slab into the deep Earth mantle and estimate the depth at which geophysical anomalies caused by carbonated eclogitic slab may occur (Supplementary Data 3). On the other hand, the impact of the iron content in eclogites on the carbon carrying capacity and the potential geophysical anomalies of carbonated eclogitic slab cannot be ignored[126]. Therefore, we chose two types of eclogites for this calculation: high-Fe (this study) and low-Fe (MORB) eclogites (Supplementary Figs. 8 and 9). Additionally, we selected six natural carbonated eclogites from the Dabie-sulu and Western Tianshan UHP/UHPM belts after complete dehydration as dry carbonated eclogites to calculate their density and velocity in the hottest and coldest subduction zones in comparison with our lab-constituted carbonated eclogites (Supplementary Figs. 8 and 9). H146-3* and 11RC-8E* are two natural carbonated eclogites from the Dabie-sulu and Western Tianshan UHP/UHPM belts before dehydration to participate in the calculations for comparison with dry carbonated eclogites (Supplementary Figs. 8 and 9).

## Data availability

The datasets of the electrical conductivity measurement supporting the finding of this study are available at https://doi.org/10.6084/m9.figshare.23559903.

## Code availability

The open-sourced software Perple_X and thermodynamic data can be downloaded from http://www.perplex.ethz.ch/.

Received: 21 July 2022; Accepted: 19 July 2023;
Published online: 29 July 2023

## References

1. Muller, R. D. et al. Evolution of Earth's tectonic carbon conveyor belt. *Nature* **605**, 629–639 (2022).
2. Kelemen, P. B. & Manning, C. E. Reevaluating carbon fluxes in subduction zones, what goes down, mostly comes up. *Proc. Natl Acad. Sci. USA* **112**, E3997–E4006 (2015).
3. Plank, T. & Manning, C. E. Subducting carbon. *Nature* **574**, 343–352 (2019).
4. Dasgupta, R. & Hirschmann, M. M. The deep carbon cycle and melting in Earth's interior. *Earth Planet. Sci. Lett.* **298**, 1–13 (2010).
5. Piccoli, F. et al. Carbonation by fluid–rock interactions at high-pressure conditions: implications for carbon cycling in subduction zones. *Earth Planet. Sci. Lett.* **445**, 146–159 (2016).
6. Farsang, S. et al. Deep carbon cycle constrained by carbonate solubility. *Nat. Commun.* **12**, 4311 (2021).
7. Dasgupta, R. et al. Carbon-dioxide-rich silicate melt in the Earth's upper mantle. *Nature* **493**, 211–215 (2013).
8. Chen, C., Förster, M. W., Foley, S. F. & Liu, Y. Massive carbon storage in convergent margins initiated by subduction of limestone. *Nat. Commun.* **12**, 4463 (2021).
9. Aiuppa, A., Casetta, F., Coltorti, M., Stagno, V. & Tamburello, G. Carbon concentration increases with depth of melting in Earth's upper mantle. *Nat. Geosci.* **14**, 697–703 (2021).
10. Stewart, E. et al. Carbonation and decarbonation reactions: implications for planetary habitability. *Am. Mineral* **104**, 1369–1380 (2019).
11. Gonzalez, C. M., Gorczyk, W. & Gerya, T. V. Decarbonation of subducting slabs: Insight from petrological–thermomechanical modeling. *Gondwana Res.* **36**, 314–332 (2016).
12. Antonelli, M. A. et al. Calcium isotope evidence for early Archaean carbonates and subduction of oceanic crust. *Nat. Commun.* **12**, 2534 (2021).
13. Cerantola, V. et al. Stability of iron-bearing carbonates in the deep Earth's interior. *Nat. Commun.* **8**, 15960 (2017).
14. Okamoto, A. et al. Rupture of wet mantle wedge by self-promoting carbonation. *Commun. Earth Environ.* **2**, 151 (2021).
15. Tao, R. & Fei, Y. Recycled calcium carbonate is an efficient oxidation agent under deep upper mantle conditions. *Commun. Earth Environ.* **2**, 45 (2021).
16. Lv, M. et al. Reversal of carbonate-silicate cation exchange in cold slabs in Earth's lower mantle. *Nat. Commun.* **12**, 1712 (2021).
17. Stewart, E. M. & Ague, J. J. Pervasive subduction zone devolatilization recycles $CO_2$ into the forearc. *Nat. Commun.* **11**, 6220 (2020).
18. Regier, M. E. et al. The lithospheric-to-lower-mantle carbon cycle recorded in superdeep diamonds. *Nature* **585**, 234–238 (2020).
19. Horton, F. Rapid recycling of subducted sedimentary carbon revealed by Afghanistan carbonatite volcano. *Nat. Geosci.* **14**, 508–512 (2021).
20. Gillis, K. M. & Coogan, L. A. Secular variation in carbon uptake into the ocean crust. *Earth Planet. Sci. Lett.* **302**, 385–392 (2011).
21. Gorman, P. J., Kerrick, D. M. & Connolly, J. A. D. Modeling open system metamorphic decarbonation of subducting slabs. *Geochem. Geophys. Geosyst.* **7** https://doi.org/10.1029/2005GC001125 (2006).
22. Merdith, A. S., Atkins, S. E. & Tetley, M. G. Tectonic controls on carbon and serpentinite storage in subducted upper oceanic lithosphere for the past 320 Ma. *Front. Earth Sci.* **7**, 332 (2019).
23. Semprich, J., Filiberto, J., Treiman, A. H. & Schwenzer, S. P. Constraints on the formation of carbonates and low-grade metamorphic phases in the Martian crust as a function of H2O-CO2 fluids. *Meteorit. Planet. Sci.* **57**, 77–104 (2021).
24. Ague, J. J. & Nicolescu, S. Carbon dioxide released from subduction zones by fluid-mediated reactions. *Nat. Geosci.* **7**, 355–360 (2014).
25. Peng, W. et al. Abiotic methane generation through reduction of serpentinite-hosted dolomite: implications for carbon mobility in subduction zones. *Geochim. Cosmochim. Acta* **311**, 119–140 (2021).
26. Xu, M. et al. High-pressure elastic properties of dolomite melt supporting carbonate-induced melting in deep upper mantle. *Proc. Natl Acad. Sci. USA* **117**, 18285–18291 (2020).
27. Hou, M. et al. Temperature-induced amorphization in CaCO3 at high pressure and implications for recycled CaCO3 in subduction zones. *Nat. Commun.* **10**, 1963 (2019).
28. Zhang, Z., Mao, Z., Liu, X., Zhang, Y. & Brodholt, J. Stability and reactions of $CaCO_3$ polymorphs in the Earth's deep mantle. *J. Geophys. Res. Solid Earth* **123**, 6491–6500 (2018).
29. Tao, R., Zhang, L. & Zhang, L. Redox evolution of western Tianshan subduction zone and its effect on deep carbon cycle. *Geosci. Front.* **11**, 915–924 (2020).
30. Zhu, J., Zhang, L., Lü, Z. & Bader, T. Elemental and isotopic (C, O, Sr, Nd) compositions of Late Paleozoic carbonated eclogite and marble from the SW Tianshan UHP belt, NW China: implications for deep carbon cycle. *J. Asian Earth Sci.* **153**, 307–324 (2018).
31. Li, J., Klemd, R., Gao, J. & Meyer, M. Coexisting carbonate-bearing eclogite and blueschist in SW Tianshan, China: petrology and phase equilibria. *J. Asian Earth Sci.* **60**, 174–187 (2012).
32. Tao, R., Zhang, L., Li, S., Zhu, J. & Ke, S. Significant contrast in the Mg-C-O isotopes of carbonate between carbonated eclogite and marble from the S.W. Tianshan UHP subduction zone: evidence for two sources of recycled carbon. *Chem. Geol.* **483**, 65–77 (2018).
33. Lappin, M. & Smith, D. Mantle-equilibrated orthopyroxene eclogite pods from the basal gneisses in the Selje district, western Norway. *J. Petrol.* **19**, 530–584 (1978).

34. Mukherjee, B. K., Sachan, H. K., Ogasawara, Y., Muko, A. & Yoshioka, N. Carbonate-bearing UHPM rocks from the Tso-Morari Region, Ladakh, India: petrological implications. *Int. Geol. Rev.* **45**, 49–69 (2003).
35. Holland, T. High water activities in the generation of high pressure kyanite eclogites of the Tauern Window, Austria. *J. Geol.* **87**, 1–27 (1979).
36. Zhu, J., Zhang, L., Tao, R. & Fei, Y. The formation of graphite-rich eclogite vein in S.W. Tianshan (China) and its implication for deep carbon cycling in subduction zone. *Chem. Geol.* **533**, 119430 (2020).
37. Kwon, S. et al. Eclogite resembling metamorphic disequilibrium assemblage formed through fluid-induced metasomatic reactions. *Sci. Rep.* **10**, 19869 (2020).
38. Xu, C. et al. Cold deep subduction recorded by remnants of a Paleoproterozoic carbonated slab. *Nat. Commun.* **9**, 2790 (2018).
39. Klemd, R. Ultrahigh-pressure metamorphism in eclogites from the western Tianshan high-pressure belt (Xinjiang, western China)—Comment. *Am. Mineral.* **88**, 1153–1156 (2003).
40. Zhang, R. & Liou, J. Significance of magnesite paragenesis in ultrahigh-pressure metamorphic rocks. *Am. Mineral.* **79**, 397–400 (1994).
41. Wang, S., Teng, F. & Li, S. Tracing carbonate-silicate interaction during subduction using magnesium and oxygen isotopes. *Nat. Commun.* **5**, 5328 (2014).
42. Hammouda, T. High-pressure melting of carbonated eclogite and experimental constraints on carbon recycling and storage in the mantle. *Earth Planet. Sci. Lett.* **214**, 357–368 (2003).
43. Dasgupta, R., Hirschmann, M. M. & Withers, A. C. Deep global cycling of carbon constrained by the solidus of anhydrous, carbonated eclogite under upper mantle conditions. *Earth Planet. Sci. Lett.* **227**, 73–85 (2004).
44. Yaxley, G. M. & Brey, G. P. Phase relations of carbonate-bearing eclogite assemblages from 2.5 to 5.5 GPa: implications for petrogenesis of carbonatites. *Contrib. Mineral. Petrol.* **146**, 606–619 (2004).
45. Kiseeva, E. S. et al. An experimental study of carbonated eclogite at 3.5-5.5 GPa—implications for silicate and carbonate metasomatism in the cratonic mantle. *J. Petrol.* **53**, 727–759 (2012).
46. Thomson, A. R., Walter, M. J., Kohn, S. C. & Brooker, R. A. Slab melting as a barrier to deep carbon subduction. *Nature* **529**, 76–79 (2016).
47. Li, J., Klemd, R., Gao, J. & Meyer, M. Compositional zoning in dolomite from lawsonite-bearing eclogite (SW Tianshan, China): evidence for prograde metamorphism during subduction of oceanic crust. *Am. Mineral.* **99**, 206–217 (2014).
48. Dasgupta, R., Hirschmann, M. M. & Dellas, N. The effect of bulk composition on the solidus of carbonated eclogite from partial melting experiments at 3 GPa. *Contrib. Mineral. Petrol.* **149**, 288–305 (2005).
49. Gaillard, F., Malki, M., Iacono-Marziano, G., Pichavant, M. & Scaillet, B. Carbonatite melts and electrical conductivity in the asthenosphere. *Science* **322**, 1363–1365 (2008).
50. Yoshino, T., Laumonier, M., McIsaac, E. & Katsura, T. Electrical conductivity of basaltic and carbonatite melt-bearing peridotites at high pressures: implications for melt distribution and melt fraction in the upper mantle. *Earth Planet. Sci. Lett.* **295**, 593–602 (2010).
51. Yoshino, T., McIsaac, E., Laumonier, M. & Katsura, T. Electrical conductivity of partial molten carbonate peridotite. *Phys. Earth Planet. Inter.* **194-195**, 1–9 (2012).
52. Yoshino, T., Gruber, B. & Reinier, C. Effects of pressure and water on electrical conductivity of carbonate melt with implications for conductivity anomaly in continental mantle lithosphere. *Phys. Earth Planet. Inter.* **281**, 8–16 (2018).
53. Karato, S. Some notes on hydrogen-related point defects and their role in the isotope exchange and electrical conductivity in olivine. *Phys. Earth Planet. Inter.* **248**, 94–98 (2015).
54. Han, K., Guo, X., Zhang, J., Wang, X. & Clark, S. M. Fast grain-boundary ionic conduction in multiphase aggregates as revealed by electrical conductivity measurements. *Contrib. Mineral. Petrol.* **176**, 1–19 (2021).
55. Liu, H., Zhang, K., Ingrin, J. & Yang, X. Electrical conductivity of omphacite and garnet indicates limited deep water recycling by crust subduction. *Earth Planet. Sci. Lett.* **559**, 116784 (2021).
56. Li, Z., Li, J., Lange, R., Liu, J. & Militzer, B. Determination of calcium carbonate and sodium carbonate melting curves up to Earth's transition zone pressures with implications for the deep carbon cycle. *Earth Planet. Sci. Lett.* **457**, 395–402 (2017).
57. Solopova, N. A., Dubrovinsky, L., Spivak, A. V., Litvin, Y. A. & Dubrovinskaia, N. Melting and decomposition of MgCO3 at pressures up to 84 GPa. *Phys. Chem. Miner.* **42**, 73–81 (2014).
58. Dong, J., Li, J., Zhu, F., Li, Z. & Farawi, R. Melting curve minimum of barium carbonate BaCO3 near 5 GPa. *Am. Mineral.* **104**, 671–678 (2019).
59. Ghosh, S., Ohtani, E., Litasov, K. D. & Terasaki, H. Solidus of carbonated peridotite from 10 to 20 GPa and origin of magnesiocarbonatite melt in the Earth's deep mantle. *Chem. Geol.* **262**, 17–28 (2009).
60. Dasgupta, R. H. & Marc, M. Effect of variable carbonate concentration on the solidus of mantle peridotite. *Am. Mineral.* **92**, 370–379 (2007).
61. Irving, A. J. & Wyllie, P. J. Subsolidus and melting relationships for calcite, magnesite and the join CaCO3-MgCO3 36 kb. *Geochim. Cosmochim. Acta* **39**, 35–53 (1975).
62. Shatskiy, A. et al. Revision of the $CaCO_3$–$MgCO_3$ phase diagram at 3 and 6 GPa. *Am. Mineral* **103**, 441–452 (2018).
63. Franzolin, E., Schmidt, M. W. & Poli, S. Ternary Ca–Fe–Mg carbonates: subsolidus phase relations at 3.5 GPa and a thermodynamic solid solution model including order/disorder. *Contrib. Mineral. Petrol.* **161**, 213–227 (2010).
64. Mityaev, A. S., Safonov, O. G., Varlamov, D. A. & van Reenen, D. D. Partial melting of carbonate–biotite gneiss at the conditions of the continental crust: experimental and thermodynamic modeling. *Petrology* **30**, 278–304 (2022).
65. Arefiev, A. V., Shatskiy, A., Podborodnikov, I. V., Bekhtenova, A. & Litasov, K. D. The system $K_2CO_3$-$CaCO_3$-$MgCO_3$ at 3 GPa: implications for carbonatite melt compositions in the shallow continental lithosphere. *Minerals* **9**, 296 (2019).
66. Shatskiy, A. et al. Phase relations in the system $FeCO_3$-$CaCO_3$ at 6 GPa and 900-1700 C and its relation to the system CaCO3-$FeCO_3$-$MgCO_3$. *Am. Mineral.* **99**, 773–785 (2014).
67. Tao, R., Zhang, L., Fei, Y. & Liu, Q. The effect of Fe on the stability of dolomite at high pressure: experimental study and petrological observation in eclogite from southwestern Tianshan, China. *Geochim. Cosmochim. Acta* **143**, 253–267 (2014).
68. Zhao, C., Xu, L., Gui, W. & Liu, J. Phase stability and vibrational properties of iron-bearing carbonates at high pressure. *Minerals* **10**, 1142 (2020).
69. Mao, Z. et al. Dolomite III: a new candidate lower mantle carbonate. *Geophys. Res. Lett.* **38**, L22303 (2011).
70. Wang, F., Zhao, C., Xu, L. & Liu, J. Effects of hydrostaticity and Mn-substitution on dolomite stability at high pressure. *Am. Mineral.* **107**, 2234–2241 (2022).
71. Antao, S. M., Mulder, W. H., Hassan, I., Crichton, W. A. & Parise, J. B. Cation disorder in dolomite, CaMg (CO3) 2, and its influence on the aragonite+ magnesite↔ dolomite reaction boundary. *Am. Mineral.* **89**, 1142–1147 (2004).
72. Franzolin, E., Merlini, M., Poli, S. & Schmidt, M. W. The temperature and compositional dependence of disordering in Fe-bearing dolomites. *Am. Mineral.* **97**, 1676–1684 (2012).
73. Hong, L., Xu, Y., Zhang, L., Wang, Y. & Ma, L. Recycled carbonate-induced oxidization of the convective mantle beneath Jiaodong, Eastern China. *Lithos* **366**, 105544 (2020).
74. Zhang, Z., You, Z., Han, Y. & Sang, L. Petrology, metamorphic process and genesis of the Dabie—Sulu Eclogite Belt, Eastern—Central China. *Acta Geol. Sin.* **9**, 134–156 (1996).
75. Omori, S., Liou, J., Zhang, R. & Ogasawara, Y. Petrogenesis of impure dolomitic marble from the Dabie Mountains, central China. *Isl. Arc.* **7**, 98–114 (1998).
76. Liu, F., Gerdes, A., Liou, J., Xue, H. & Liang, F. SHRIMP U-Pb zircon dating from Sulu-Dabie dolomitic marble, eastern China: constraints on prograde, ultrahigh-pressure and retrograde metamorphic ages. *J. Metamorph. Geol.* **24**, 569–589 (2006).
77. Dai, L. & Karato, S. Electrical conductivity of Ti-bearing hydrous olivine aggregates at high temperature and high pressure. *J. Geophys. Res. Solid Earth* **125**, e2020JB020309 (2020).
78. Fei, H. & Katsura, T. The effect of oxygen fugacity on ionic conductivity in olivine. *Geosci. Front.* **13**, 101270 (2022).
79. Ono, S. & Mibe, K. Influence of pressure and temperature on the electrical conductivity of dolomite. *Phys. Chem. Miner.* **42**, 773–779 (2015).
80. Ono, S. & Mibe, K. Electrical conductivity of aragonite in the subducted slab. *Eur. J. Mineral.* **25**, 11–15 (2013).
81. Mibe, K. & Ono, S. Electrical conductivity of $MgCO_3$ at high pressures and high temperatures. *Phys. B* **406**, 2018–2020 (2011).
82. Sanchez-Valle, C., Ghosh, S. & Rosa, A. D. Sound velocities of ferromagnesian carbonates and the seismic detection of carbonates in eclogites and the mantle. *Geophys. Res. Lett.* **38**, L24315 (2011).
83. Stekiel, M. et al. High pressure elasticity of $FeCO_3$-$MgCO_3$ carbonates. *Phys. Earth Planet. Inter.* **271**, 57–63 (2017).
84. Li, Y. et al. Sound velocity of aragonite ($CaCO_3$) at high pressure and high temperature and implications for low velocity zone in the subduction zone. *Earth Space Sci. Open Arch.* https://doi.org/10.1002/essoar.10508650.10508651 (2021).
85. Litasov, K. D. et al. P-V-T equation of state of $CaCO_3$ aragonite to 29 GPa and 1673 K: in situ X-ray diffraction study. *Phys. Earth Planet. Inter.* **265**, 82–91 (2017).
86. Herzberg, C. Understanding the paleoproterozoic circum-superior large igneous province constrains the thermal properties of Earth's mantle through time. *Precambrian Res.* **375**, 106671 (2022).
87. Lucas, E. M. et al. Shear wave splitting across Antarctica: implications for upper mantle seismic anisotropy. *J. Geophys. Res. Solid Earth* **127**, e2021JB023325 (2022).

88. Wilson, A. & Bolhar, R. Olivine in komatiite records origin and travel from the deep upper mantle. *Geology* **50**, 351–355 (2021).
89. Sun, M. et al. Exploring small-scale recycled mantle components with intraplate continental twin volcanoes. *Chem. Geol.* **598**, 120842 (2022).
90. Xu, J. et al. Phase transition of enstatite-ferrosilite solid solutions at high pressure and high temperature: constraints on metastable orthopyroxene in cold subduction. *Geophys. Res. Lett.* **47**, e2020GL087363 (2020).
91. Wang, S. & Zhang, G. Geochemical constraints on source nature and recycled oceanic crust in the mantle of the Celebes Sea. *Lithos* **418**, 106685 (2022).
92. Hsieh, W. P., Marzotto, E., Tsao, Y. C., Okuchi, T. & Lin, J. High thermal conductivity of stishovite promotes rapid warming of a sinking slab in Earth's mantle. *Earth Planet. Sci. Lett.* **584**, 117477 (2022).
93. Ballmer, M. D., Schmerr, N. C., Nakagawa, T. & Ritsema, J. Compositional mantle layering revealed by slab stagnation at~ 1000-km depth. *Sci. Adv.* **1**, e1500815 (2015).
94. Kong, F. et al. Metastable olivine within oceanic lithosphere in the uppermost lower mantle beneath the eastern United States. *Geology* **50**, 776–780 (2022).
95. Arora, B. R., Unsworth, M. J. & Rawat, G. Deep resistivity structure of the northwest Indian Himalaya and its tectonic implications. *Geophys. Res. Lett.* **34**, L04307 (2007).
96. Bielinski, R. A. et al. Lithospheric heterogeneity in the Kyrgyz Tien Shan imaged by magnetotelluric studies. *Geophys. Res. Lett.* **30**, 1806 (2003).
97. Xiao, Q. et al. A preliminary study on electrical structure and dynamics of the ultra-high pressure metamorphic belt beneath the Dabie Mountains. *Chin. J. Geophys.* **50**, 710–721 (2007).
98. Jeppson, T. N. & Kitajima, H. Velocity-porosity relations in carbonate and siliciclastic subduction zone input materials. *Geochem. Geophys. Geosyst.* **23**, e2021GC010074 (2021).
99. Sun, W. et al. Carbonated mantle domains at the base of the Earth's transition zone. *Chem. Geol.* **478**, 69–75 (2018).
100. Yang, J., Wu, W., Lian, D. & Rui, H. Peridotites, chromitites and diamonds in ophiolites. *Nat. Rev. Earth Environ.* **2**, 198–212 (2021).
101. Chantel, J., Mookherjee, M. & Frost, D. J. The elasticity of lawsonite at high pressure and the origin of low velocity layers in subduction zones. *Earth Planet. Sci. Lett.* **349-350**, 116–125 (2012).
102. Cai, N. et al. Enhanced visibility of subduction slabs by the formation of dense hydrous phase A. *Geophys. Res. Lett.* **48**, e2021GL095487 (2021).
103. Stern, R. J. Subduction zones. *Rev. Geophys.* **40**, 3-1-3-38 (2002).
104. Peacock, S. M. Thermal and petrologic structure of subduction zones. In: *Subduction: Top to Bottom* (eds. Bebout G. E., Scholl D. W., Kirby S. H., Platt J. P.), Vol. 96, 119–133 (1996).
105. Yang, X. & Heidelbach, F. Grain size effect on the electrical conductivity of clinopyroxene. *Contrib. Mineral. Petrol.* **163**, 939–947 (2011).
106. Pommier, A. et al. Transport properties of olivine grain boundaries from electrical conductivity experiments. *Contrib. Mineral. Petrol.* **173**, 1–13 (2018).
107. McCammon, C. The paradox of mantle redox. *Science* **308**, 807–808 (2005).
108. Dai, L. & Karato, S.-I. Electrical conductivity of pyrope-rich garnet at high temperature and high pressure. *Phys. Earth Planet. Inter.* **176**, 83–88 (2009).
109. Wang, D., Mookherjee, M., Xu, Y. & Karato, S. The effect of water on the electrical conductivity of olivine. *Nature* **443**, 977–980 (2006).
110. Sheng, Y., Xia, Q., Dallai, L., Yang, X. & Hao, Y. H2O contents and D/H ratios of nominally anhydrous minerals from ultrahigh-pressure eclogites of the Dabie orogen, eastern China. *Geochim. Cosmochim. Acta* **71**, 2079–2103 (2007).
111. Zhang, B., Zhao, C., Ge, J. & Yoshino, T. Electrical conductivity of omphacite as a function of water content and implications for high conductivity anomalies in the Dabie-Sulu UHPM Belts and Tibet. *J. Geophys. Res. Solid Earth* **124**, 12523–12536 (2019).
112. Liu, H., Zhu, Q. & Yang, X. Electrical conductivity of OH-bearing omphacite and garnet in eclogite: the quantitative dependence on water content. *Contrib. Mineral. Petrol.* **174**, 1–15 (2019).
113. Katayama, I., Nakashima, S. & Yurimoto, H. Water content in natural eclogite and implication for water transport into the deep upper mantle. *Lithos* **86**, 245–259 (2006).
114. Droop, G. T. R. A general equation for estimating $Fe^{3+}$ concentrations in ferromagnesian silicates and oxides from microprobe analyses, using stoichiometric criteria. *Mineral. Mag.* **51**, 431–435 (1987).
115. Connolly, J. A. D. Computation of phase equilibria by linear programming: a tool for geodynamic modeling and its application to subduction zone decarbonation. *Earth Planet. Sci. Lett.* **236**, 524–541 (2005).
116. Holland, T. J. B. & Powell, R. An internally consistent thermodynamic data set for phases of petrological interest. *J. Metamorph. Geol* **16**, 309–343 (1998).
117. Holland, T. & Powell, R. Thermodynamics of order-disorder in minerals; I, Symmetric formalism applied to minerals of fixed composition. *Am. Mineral.* **81**, 1413–1424 (1996).
118. Andersen, D. J. & Lindsley, D. H. Internally consistent solution models for Fe-Mg-Mn-Ti oxides-Fe-Ti oxides. *Am. Mineral.* **73**, 714–726 (1988).
119. Anovitz, L. M. & Essene, E. J. Phase equilibria in the system $CaCO_3$-$MgCO_3$-$FeCO_3$. *J. Petrol.* **28**, 389–415 (1987).
120. Dale, J., Powell, R., White, R. W., Elmer, F. L. & Holland, T. J. B. A thermodynamic model for Ca-Na clinoamphiboles in $Na_2O$-CaO-FeO-MgO-$Al_2O_3$-$SiO_2$-$H_2O$-O for petrological calculations. *J. Metamorph. Geol.* **23**, 771–791 (2005).
121. Holland, T. & Powell, R. A compensated-Redlich-Kwong (CORK) equation for volumes and fugacities of $CO_2$ and $H_2O$ in the range 1 bar to 50 kbar and 100–1600 C. *Contrib. Mineral. Petrol.* **109**, 265–273 (1991).
122. Syracuse, E. M., van Keken, P. E. & Abers, G. A. The global range of subduction zone thermal models. *Phys. Earth Planet. Inter.* **183**, 73–90 (2010).
123. Penniston-Dorland, S. C., Kohn, M. J. & Manning, C. E. The global range of subduction zone thermal structures from exhumed blueschists and eclogites: rocks are hotter than models. *Earth Planet. Sci. Lett.* **428**, 243–254 (2015).
124. Aoki, I. & Takahashi, E. Density of MORB eclogite in the upper mantle. *Phys. Earth Planet. Inter.* **143**, 129–143 (2004).
125. Chen, Y., Ye, K., Wu, T. & Guo, S. Exhumation of oceanic eclogites: thermodynamic constraints on pressure, temperature, bulk composition and density. *J. Metamorph. Geol.* **31**, 549–570 (2013).
126. Xu, J. et al. Thermoelastic properties of eclogitic garnets and omphacites: implications for deep subduction of oceanic crust and density anomalies in the upper mantle. *Geophys. Res. Lett.* **46**, 179–188 (2019).
127. Ye, Z. et al. Thermal equation of state of the main minerals of eclogite: constraining the density evolution of eclogite during the delamination process in Tibet. *Solid Earth* **13**, 745–759 (2022).
128. Wang, Y., Zhang, L. F., Li, Z. H., Li, Q. Y. & Bader, T. The exhumation of subducted oceanic-derived eclogites: insights from phase equilibrium and thermomechanical modeling. *Tectonics* **38**, 1764–1797 (2019).
129. Konilov, A. N. et al. The Salma eclogites of the Belomorian Province, Russia: HP/UHP metamorphism through the subduction of Mesoarchean oceanic crust. In: *Ultrahigh-Pressure Metamorphism* (eds. Dobrzhinetskaya L. F., Faryad S. W., Wallis S., Cuthbert S.), (Elsevier, 2011).
130. Mints, M. V., Dokukina, K. A. & Konilov, A. N. The Meso-Neoarchaean Belomorian eclogite province: tectonic position and geodynamic evolution. *Gondwana Res.* **25**, 561–584 (2014).
131. Pertermann, M. & Hirschmann, M. M. Partial melting experiments on a MORB-like pyroxenite between 2 and 3 GPa: constraints on the presence of pyroxenite in basalt source regions from solidus location and melting rate. *J. Geophys. Res. Solid Earth* **108**, 2125 (2003).
132. Dziewonski, A. M. & Anderson, D. L. Preliminary reference Earth model. *Phys. Earth Planet. Inter.* **25**, 297–356 (1981).
133. Nishi, M., Kubo, T. & Kato, T. Metastable transformations of eclogite to garnetite in subducting oceanic crust. *J. Mineral. Petrol. Sci.* **104**, 192–198 (2009).
134. Cammarano, F., Goes, S., Vacher, P. & Giardini, D. Inferring upper-mantle temperatures from seismic velocities. *Phys. Earth Planet. Inter.* **138**, 197–222 (2003).
135. Xu, W., Lithgow-Bertelloni, C., Stixrude, L. & Ritsema, J. The effect of bulk composition and temperature on mantle seismic structure. *Earth Planet. Sci. Lett.* **275**, 70–79 (2008).
136. Chapman, D. S. Thermal gradients in the continental crust. Geological Society, London, Special Publications 24, 63–70 (1986).
137. Katsura, T., Baba, K., Yoshino, T. & Kogiso, T. Electrical conductivity of the oceanic asthenosphere and its interpretation based on laboratory measurements. *Tectonophysics* **717**, 162–181 (2017).
138. Kelbert, A., Schultz, A. & Egbert, G. Global electromagnetic induction constraints on transition-zone water content variations. *Nature* **460**, 1003–1006 (2009).
139. Baba, K. et al. Electrical conductivity imaging of the Philippine Sea upper mantle using seafloor magnetotelluric data. *Phys. Earth Planet. Inter.* **183**, 44–62 (2010).
140. Tsujimori, T. & Mattinson, C. Eclogites in Different Tectonic Settings. In: *Encyclopedia of Geology (Second Edition)* (eds. Alderton D., Elias S. A.). (Academic Press, 2021).
141. Stern, R. J. A subduction primer for instructors of introductory-geology courses and authors of introductory-geology textbooks. *J. Geosci. Educ.* **46**, 221–228 (1998).
142. Eberhard, L. *Serpentinite Phase Relations—An Experimental Study on Redox Conditions and Fluid Migration in Subduction Z*ones (Universität Bayreuth, Fakultät für Biologie, Chemie und Geowissenschaften, 2021).
143. Scicchitano, M. R., Lafay, R., Valley, J. W., Kita, N. T. & Nachlas, W. O. Protracted hydrothermal alteration recorded at the microscale in the Chenaillet ophicarbonates (Western Alps): Insights from in situ δ18O thermometry in serpentine, carbonate and magnetite. *Geochim. Cosmochim. Acta* **318**, 144–164 (2022).
144. Steele, A. et al. Organic synthesis associated with serpentinization and carbonation on early Mars. *Science* **375**, 172–177 (2022).
145. Smith, E. M. et al. Heavy iron in large gem diamonds traces deep subduction of serpentinized ocean floor. *Sci. Adv.* **7**, eabe9773 (2021).

146. Scambelluri, M. et al. Carbonation of subduction-zone serpentinite (high-pressure ophicarbonate; Ligurian Western Alps) and implications for the deep carbon cycling. *Earth Planet. Sci. Lett.* **441**, 155–166 (2016).
147. Alt, J. C. & Teagle, D. A. The uptake of carbon during alteration of ocean crust. *Geochim. Cosmochim. Acta* **63**, 1527–1535 (1999).
148. Kerrick, D. M. & Connolly, J. A. D. Metamorphic devolatilization of subducted oceanic metabasalts: implications for seismicity, arc magmatism and volatile recycling. *Earth Planet. Sci. Lett.* **189**, 19–29 (2001).
149. Alt, J. C. et al. The role of serpentinites in cycling of carbon and sulfur: Seafloor serpentinization and subduction metamorphism. *Lithos* **178**, 40–54 (2013).
150. Bekaert, D. V. et al. Subduction-driven volatile recycling: a global mass balance. *Annu. Rev. Earth Planet. Sci.* **49**, 37–70 (2021).
151. Wen, T. et al. Carbonatitic pockets in intra-ocean arc volcanics (Qilian orogen): petrogenesis and implications for carbon recycling in subduction zones. *Chem. Geol.* **606**, 120981 (2022).
152. Lai, X. et al. Melting of the Fe-C-H system and Earth's deep carbon-hydrogen cycle. *Geophys. Res. Lett.* **49**, e2022GL098919 (2022).
153. Lei, J., Sen, S., Li, Y., Zhang & Zhou, J. Carbon in the deep upper mantle and transition zone under reduced conditions: insights from high-pressure experiments and machine learning models. *Geochim. Cosmochim. Acta* **332**, 88–102 (2022).
154. Dorfman, S. M. et al. Carbonate stability in the reduced lower mantle. *Earth Planet. Sci. Lett.* **489**, 84–91 (2018).
155. Lara, M. & Dasgupta, R. Carbon recycling efficiency in subduction zones constrained by the effects of $H_2O$-$CO_2$ fluids on partial melt compositions in the mantle wedge. *Earth Planet. Sci. Lett.* **588**, 117578 (2022).
156. Dobretsov, N. L. & Shatskiy, A. F. Deep carbon cycle and geodynamics: the role of the core and carbonatite melts in the lower mantle. *Russ. Geol. Geophys* **53**, 1117–1132 (2012).
157. Poli, S. Carbon mobilized at shallow depths in subduction zones by carbonatitic liquids. *Nat. Geosci.* **8**, 633–636 (2015).
158. Elazar, O., Frost, D., Navon, O. & Kessel, R. Melting of $H_2O$ and $CO_2$-bearing eclogite at 4–6 GPa and 900–1200 °C: Implications for the generation of diamond-forming fluids. *Geochim. Cosmochim. Acta* **255**, 69–87 (2019).

## Acknowledgements

This study was financially supported by the National Natural Science Foundation of China (Grant Nos. 42274137 and 42072055) and the Youth Innovation Promotion Association of CAS (Grant No. 2019390).

## Author contributions

H.H. and C.J. designed the study. C.J. prepared the original draft under the supervision of L.D. and H.H.; C.J., W.S., W.M. and Z.H. conducted the experiments. All authors contributed to the manuscript.

## Competing interests

The authors declare no competing interests.

## Additional information

**Supplementary information** The online version contains supplementary material available at https://doi.org/10.1038/s43247-023-00936-w.

**Correspondence** and requests for materials should be addressed to Haiying Hu.

**Peer review information** *Communications Earth & Environment* thanks Pierre Lanari, Renbiao Tao and the other, anonymous, reviewer(s) for their contribution to the peer review of this work. Primary Handling Editors: Maria Luce Frezzotti and Joe Aslin. A peer review file is available.